

1 The effect of low solubility organic acids on the  
2 hygroscopicity of sodium halide aerosols

3

4 Lorena Miñambres\*, Estíbaliz Méndez, María N. Sánchez, Fernando Castaño and Francisco J.  
5 Basterretxea

6

7 *Departamento de Química Física*

8 *Facultad de Ciencia y Tecnología*

9 *University of the Basque Country, UPV/EHU*

10 *Campus de Leioa*

11 *B. Sarriena, s/n*

12 *Leioa 48940 SPAIN*

13

14

15

16

17

18

19

20

21

22

23

24 \*Corresponding author

25 Lorena Miñambres

26 Phone: +34 94 601 5386

27 Fax: +34 94 601 3500

28 E-mail address: [lorena.minambres@ehu.es](mailto:lorena.minambres@ehu.es)

29

30

31

32 **ABSTRACT**

33

34 In order to accurately assess the influence of fatty acids on the hygroscopic and other  
35 physicochemical properties of sea salt aerosols, hexanoic, octanoic or lauric acid together with  
36 sodium halide salts (NaCl, NaBr and NaI) have been chosen to be investigated in this study. The  
37 hygroscopic properties of sodium halide submicrometer particles covered with organic acids have  
38 been examined by Fourier-transform infrared spectroscopy in an aerosol flow cell. Covered  
39 particles were generated by flowing atomized sodium halide particles (either dry or aqueous)  
40 through a heated oven containing the gaseous acid. The obtained results indicate that gaseous  
41 organic acids easily nucleate onto dry and aqueous sodium halide particles. On the other hand,  
42 Scanning Electron Microscopy (SEM) images indicate that lauric acid coating on NaCl particles  
43 makes them to aggregate in small clusters. The hygroscopic behaviour of covered sodium halide  
44 particles in deliquescence mode shows different features with the exchange of the halide ion:  
45 whereas the organic covering has little effect in NaBr particles, NaCl and NaI covered particles  
46 change their deliquescence relative humidities, with different trends observed for each of the acids  
47 studied. In efflorescence mode, the overall effect of the organic covering is to retard the loss of  
48 water in the particles. It has been observed that the presence of gaseous water in heterogeneously  
49 nucleated particles tends to displace the cover of hexanoic acid to energetically stabilize the system.

50

51

52 **Keywords:** marine aerosol, fatty acids, heterogeneous nucleation, hygroscopicity.

53

## 54 1. INTRODUCTION

55

56 Marine aerosol is one of the most abundant types of natural particulate matter in the Earth's  
57 troposphere. Sea salt particles play an active role in the Earth's radiative balance, influence mass  
58 transfer from gaseous substances and cloud-precipitation mechanisms, contribute to the formation  
59 of cloud condensation nuclei and have highly reactive surfaces that take part in heterogeneous and  
60 multiphase chemical reactions (Andreae and Rosenfeld 2008; Carslaw et al 2010; D O'Dowd and  
61 De Leeuw 2007; Finlayson-Pitts 2003; Lewis and Schwartz 2004; Quinn and Bates 2011; Rossi  
62 2003). They also can uptake significant amounts of water, exhibiting deliquescence and  
63 efflorescence properties under atmospheric conditions (Freney et al 2009; Martin 2000; Metzger  
64 and Lelieveld 2007; Mikhailov et al 2013; Wise et al 2012), that can change the particles' phase and  
65 size, together with other interrelated physico-chemical properties: for example, water uptake  
66 increases particle size, thus favouring their sedimentation. In parallel, bigger particles increase the  
67 scattering of solar visible light, thus influencing atmospheric radiative transfer and visibility. The  
68 presence of water in atmospheric particles can also change the adsorption of trace gases and their  
69 chemical reactivity (e.g., sulfate chemistry proceeds by adsorption of gaseous SO<sub>2</sub> on aqueous  
70 particles, followed by oxidation to sulfate; this pathway is absent in crystalline particles).

71 Marine aerosol is generated either by the mechanical action of the ocean surface (primary  
72 sea-salt aerosol), or by gas-to-particle conversion processes (secondary aerosol) mainly in the form  
73 of nonsea-salt sulphate and organic species (O'Dowd et al 1997). Sodium chloride is the principal  
74 component of sea salt: typical sea water composition has  $1.05 \times 10^4$  mg/L of Na<sup>+</sup> and  $1.9 \times 10^4$  mg/L  
75 of Cl<sup>-</sup> (Lide 1994). Bromide ions are a minor component of seawater, and hence of sea salt particles,  
76 with a molar ratio of bromide to chloride of 1:650 (Lide 1994). Despite such a small contribution to  
77 the composition of sea salt particles, bromine plays a comparatively large role in tropospheric sea  
78 salt chemistry. The most important is the drop of surface-level ozone concentrations in the Arctic at  
79 polar sunrise. This is due to the tendency of Br<sup>-</sup> to segregate to the salt surface in the presence of  
80 water, substantially increasing Br/Cl surface molar ratios, and to the fact that bromide ions exhibit a  
81 higher surface reactivity than chloride (Baker 2005; Ghosal et al 2008; Zangmeister et al 2001). Sea  
82 salt particles have been shown to be the source of BrO, which is involved in catalytic cycles that  
83 destroy ozone (Finlayson-Pitts 2009; Frinak and Abbatt 2006; Hunt et al 2004; Read et al 2008;  
84 Von Glasow 2008). Although the concentrations of I<sup>-</sup> present in seawater are much smaller than  
85 those of bromine and chlorine (the molar ratio of I<sup>-</sup> to Cl<sup>-</sup> in seawater is  $\sim 1:10^6$ ), there is evidence  
86 that iodine in the marine boundary layer has an influence on ozone destruction, the oxidizing

87 capacity of the troposphere, denoxification, and particle formation (Carpenter 2003; Saiz-Lopez et  
88 al 2008). A similar role to BrO is played by IO, although its source is believed to come from marine  
89 algae (Read et al 2008). Recently advances have been made in quantifying the link between  
90 seawater chemical processes, and the production, size, and chemical composition of sea spray  
91 aerosol particles by simultaneous measurements of seawater, particle size distributions, and size-  
92 resolved single particle chemical composition in a laboratory setting reproducing the chemical  
93 complexity of sea spray aerosol, including natural seawater, breaking waves and controlled  
94 phytoplankton and heterotrophic bacteria concentrations (Ault et al 2013; Prather et al 2013). It has  
95 been shown that the mixing state of sea aerosol is sensitive to the presence of heterotrophic bacteria,  
96 that transform dissolved organic matter.

97       Organic compounds are present in marine salt aerosol in variable proportions, that may  
98 represent a large fraction of the aerosol dry mass (Cavalli et al 2004; Gantt and Meskhidze 2013;  
99 Middlebrook et al 1998). The presence of significant concentrations of organic matter in marine  
100 aerosol was detected in earlier studies (Kleefeld et al 2002; Middlebrook et al 1998; Putaud et al  
101 2000). Measures over the North Atlantic Ocean have revealed that the organic fraction contributes  
102 up to 63% to the submicrometre aerosol mass, of which about 45% is water-insoluble and 18%  
103 water-soluble (O'Dowd et al 2004). 37% hydrocarbon and 63% oxygenated hydrocarbon speciation  
104 was observed for the organic mass, indicating that at least 37% of the organic mass is produced via  
105 primary sea-spray (Ovadnevaite et al 2011a). It was found that predominantly organic particles  
106 contribute between 25 and 30% to general background marine number concentration, 35% for open  
107 ocean nucleation cases, and 60% for anthropogenically influenced cases (Bialek et al 2012). The  
108 organic fraction of marine aerosol can be highly enriched due to oceanic biological activity (Ault et  
109 al 2013; Gantt and Meskhidze 2013; O'Dowd et al 2002; Ovadnevaite et al 2011a; Rinaldi et al  
110 2010). Much of the organic fraction corresponds to water insoluble fatty acids present as surface  
111 films on particles (Donaldson and Vaida 2006; Mochida et al 2002; Tervahattu et al 2002), but also  
112 as organic carbon more homogeneously mixed with cations and anions (Ault et al 2013). Moreover,  
113 fine mode marine organic aerosol can have a size distribution independent from that of sea-salt,  
114 while coarse mode aerosols are more likely to be internally mixed with sea-salt (Gantt and  
115 Meskhidze 2013). Primary marine aerosols mixed with a surfactant can be generated by wind action  
116 on the sea surface, which is covered by a low solubility organic layer (Donaldson and Vaida 2006).  
117 Alternatively, heterogeneously nucleated particles can form when low vapor pressure organic  
118 vapors condense on pre-existing aerosol particles, forming a surface coating, that can be evenly or  
119 unevenly distributed. It has been proposed that the organic compounds arrange in a hydrophobic  
120 organic monolayer that encapsulates an aqueous particle, forming an “inverted micelle” structure

121 (Ellison et al 1999). This model shows agreement with recent molecular dynamic simulation results  
122 (Chakraborty and Zachariah 2008). Other models predict that certain fatty acids form pockets of  
123 micelles within the aerosol, modifying the surface tension of the particle and therefore changing the  
124 water uptake properties of atmospheric aerosols (Tabazadeh 2005), and that core-shell structures are  
125 not always the most stable (Kwamena et al 2010), again affecting the particle water uptake  
126 properties and optical properties.

127         The presence of an organic film at the surface of a particle may affect its physical and  
128 chemical properties in a number of ways. The film may act as a barrier to transport across the  
129 interface, inhibiting uptake of atmospheric gases or reactions between gas phase reactants and  
130 particle surface, such as the heterogeneous reaction  $\text{NaCl(s)} + 2\text{NO}_2(\text{g}) \rightarrow \text{ClNO}(\text{g}) + \text{NaNO}_3(\text{s})$   
131 (Donaldson and Vaida 2006; Finlayson-Pitts 2003). In particular, the surface film can affect the  
132 process of cloud condensation nuclei formation and growth (Andrews and Larson 1993; Chuang  
133 2003). Organic compounds can also change the amount of light scattered by inorganic particles  
134 (Dall'Osto et al 2010; Fierz-Schmidhauser et al 2010; Vaishya et al 2013). Marine primary organic  
135 aerosol (POA) can cause large local increases in the cloud condensation nuclei concentration by  
136 15% to more than 100% (O'Dowd et al 2004; Ovadnevaite et al 2011b), and the ambient mass  
137 concentration and organic mass fraction of sea-spray aerosol are related to surface ocean biological  
138 activity. Despite considerable work has been carried out in the last years, there is still much  
139 uncertainty about fundamental issues of marine , such as chemical composition, mixing state,  
140 hygroscopicity, cloud droplet activation, formation, aging and removal mechanisms (Gantt and  
141 Meskhidze 2013; ICCP 2013). Several laboratory studies about the effect of organic surfactants,  
142 such as palmitic and oleic acids, on NaCl, ammonium sulfate or mineral dust aerosol particles as a  
143 function of relative humidity have been reported employing a variety of experimental techniques,  
144 such as electrodynamic balance, infrared spectroscopy, electrical mobility, optical tweezers, cavity  
145 ring-down spectroscopy or nonlinear spectroscopy (Cwiertny et al 2008; Davies et al 2013; Dennis-  
146 Smither et al 2012; Ebben et al 2013; Garland et al 2005; Hansson et al 1998; Najera and Horn  
147 2009; Robinson et al 2013; Rossi 2003; Rubasinghege et al 2013). The general conclusions are that  
148 hygroscopic growth, deliquescence relative humidity (DRH) and efflorescence of the particles may  
149 be affected by several factors, such as coating thickness or structural arrangement of the organic  
150 film. Special effort has been carried out to study the morphology and phase partitioning of aerosol  
151 particles consisting of hydrophobic and hydrophilic phases (Ciobanu et al 2009; Kwamena et al  
152 2010; Reid et al 2011; Veghte et al 2013). On the other hand, molecular dynamics calculations are  
153 becoming a commonplace theoretical approach in atmospheric aerosol modeling, that includes sea

154 salt particles mixed with organic molecules (Ma et al 2011; Sun et al 2012; Sun et al 2013;  
155 Takahama and Russell 2011).

156 As a whole, laboratory studies on inorganic particles coated with surfactant organics have  
157 mainly focused on a few organic molecules, and most of them have been carried out with  
158 ammonium sulfate or sodium chloride. Very few studies of hygroscopic behavior have been carried  
159 out on particles containing bromide or iodide. Furthermore, sodium chloride, bromide and iodide  
160 particles exhibit very different hygroscopic properties and interact differently with water soluble  
161 dicarboxylic acids such as succinic acid (Minambres et al 2011). It has been reported that rates of  
162 gaseous iodine emissions during the heterogeneous reaction of O<sub>3</sub> with interfacial iodide are  
163 enhanced several-fold by the presence of alkanolic acids on water, such as octanoic and hexanoic  
164 acid (Hayase et al 2011). In the present work we study the hygroscopic properties of NaX (X=Cl,  
165 Br, I) sodium halide salts coated with either one of three different surfactant carboxylic acid  
166 molecules by Fourier-transform infrared extinction spectroscopy in an aerosol flow tube, aided by  
167 particle sizing methods. The examined acids, all contain one carboxylic group at the end of the  
168 molecule, are hexanoic (CH<sub>3</sub>(CH<sub>2</sub>)<sub>4</sub>COOH), octanoic (CH<sub>3</sub>(CH<sub>2</sub>)<sub>6</sub>COOH) and dodecanoic or lauric  
169 acid (CH<sub>3</sub>(CH<sub>2</sub>)<sub>10</sub>COOH), hereafter shortened as HA, OA and LA, respectively. These acids belong  
170 to the family of alkanolic acids, that make a significant proportion of the organic compounds emitted  
171 from several sources to the atmosphere, such as seed oil and meat cooking procedures or emission  
172 by plants. HA, OA and LA have been observed in the atmosphere of remote marine and continental  
173 locations (Duce et al 1983; Gill et al 1983; Limbeck and Puxbaum 1999; Samy et al 2010; Schauer  
174 et al 1999; Schauer et al 2002; Yassaa et al 2001). OA and LA exist as liquid and solid,  
175 respectively, at typical tropospheric temperatures and pressures. HA has higher vapor pressure than  
176 the atmospherically more abundant long chain acids, that may contribute more substantially to  
177 vapor phase processes. HA, OA and LA have water solubilities of 9.9, 0.68 and 0.058 g/L at 20°C,  
178 respectively (see Table 1), and have been selected as they are expected to influence the hygroscopic  
179 behaviour of sea-salt particles differently in view of their water solubilities: HA has intermediate  
180 solubility between highly soluble and highly insoluble organic acids, whereas LA, on the other end,  
181 can represent highly insoluble fatty acids, OA lying in-between. Due to their overall low water  
182 solubility, pure fatty acids are not expected to present significant intrinsic hygroscopic properties.

183 Infrared spectroscopy is a well-known sensitive technique and has been applied to the study  
184 of organic/inorganic aerosol systems (Garland et al 2005; Najera and Horn 2009). It can yield  
185 aerosol composition, water content, and particle phase. Variations in the wavenumbers and widths  
186 of spectral bands (precisely their FWHM: full width at half maximum) can also reveal information  
187 about molecular interactions in mixed systems and the formation of new species. Infrared spectra

188 have been combined with electron scanning microscopy (SEM) of particles, a technique that has  
189 been demonstrated to be useful to study the chemistry of isolated, individual particles of  
190 atmospheric relevance (Krueger et al 2003; Veghte et al 2013). A few studies have been presented  
191 describing the effects of octanoic and lauric acids on the hygroscopicity of NaCl (Hämeri et al  
192 1992; Hansson et al 1998; Wagner et al 1996). The results indicate that formation of organic  
193 surfactant layers tend to slow NaCl deliquescence rate and to slightly lower its DRH. This may  
194 affect particle size and phase, changing the amount of scattered solar radiation and also the  
195 adsorption behavior of trace gases onto particles. Molecular dynamics simulations of water vapor  
196 molecules impinging on a slab of water coated by octanoic acid film showed that the mass  
197 accommodation coefficient decreased with the degree of surface coverage of the hydrocarbon  
198 backbones (Takahama and Russell 2011).

199

200

## 201 **2. MATERIALS AND METHODS**

202

203 The configuration of the experimental setup used in this work is based on a system described  
204 previously (Minambres et al 2010), that has been modified for the present study. The main elements  
205 are depicted in Figure 1. Submicrometric particles are formed by injecting a 0.01 kg/L aqueous  
206 solution of sodium halide salts (NaCl, NaBr and NaI,  $\geq 98\%$ ) in a commercial atomizer (TSI 3076).  
207 Their relative humidity (RH) can be controlled (from 0 to around 95%) by combining two serially  
208 connected diffusion driers and a flow of N<sub>2</sub> with a controlled amount of water vapor. The inorganic  
209 particles are coated by passing the aerosol flow (1.8 L/min) through a heated cell that contains a  
210 sample of either hexanoic (99%), octanoic ( $\geq 98\%$ ), or lauric acid ( $\geq 98\%$ ). Table 1 summarises the  
211 most relevant physical properties of these acids.

212 The heating cell consists of an horizontally-set cylindrical borosilicate glass tube 30 cm long  
213 having 3 cm internal diameter, that has two smaller glass tubes (30 and 20 cm long, 1 cm int. diam.)  
214 coaxially attached at its ends. Acid sample (either liquid or solid) is placed uniformly along the  
215 central tube. The whole cell is thermally isolated by wrapping it with alumino-silicate refractory  
216 ceramic fiber. To allow for sufficient vaporization of the acid, the central tube and exit arm of the  
217 cell are heated up to 100°C by means of flexible resistors coiled around them. The temperatures at  
218 both cell locations (T<sub>1</sub> refers to the central part, T<sub>2</sub> to the exit arm, see Figure 1) are controlled by  
219 placing two K-type thermocouples at the cell outer walls. To form heterogeneously nucleated

220 particles,  $T_1$  varied from 75 to 100°C and  $T_2$  from 60 to 90°C. Higher temperatures resulted in  
221 stronger absorption bands, indicating a higher efficiency of heterogeneous nucleation, that forms a  
222 thicker coating of NaCl particles. The temperature measurement errors are estimated to be in the 4-  
223 7°C range (the higher value corresponds to the highest temperature). A prominent baseline shift was  
224 observed in all cases, in agreement with particle formation. This shift increases with  $T_1$  and  $T_2$ ,  
225 indicating bigger particles. Purely homogeneously nucleated particles were formed by passing a  
226 flow of gaseous nitrogen through the heated oven at  $T_1=80-100^\circ\text{C}$  and  $T_2=60-90^\circ\text{C}$  containing the  
227 carboxylic acid. This coating method can get a reproducible amount of fatty acid on particles in a  
228 fast and convenient way, and has been used by other authors in laboratory experiments (Abbatt et  
229 al 2005; Garland et al 2008; Garland et al 2005; Rouviere and Ammann 2010; Stemmler et al 2008)  
230 Although in the troposphere the whole process of heterogeneous nucleation of organic vapors takes  
231 place at overall lower temperatures, in our experiment the heated organic vapor gets in contact with  
232 the nitrogen gas flow at ambient temperature, that effectively cools the vapor by rapid heat  
233 exchange (the number density of nitrogen molecules in the gas flow is much higher than the number  
234 density of organic vapor molecules in the tube). Eventually, cooled gas-phase organic molecules  
235 heterogeneously nucleate on salt particles in the nitrogen gas flow. In that way, the way to generate  
236 heterogeneously nucleated particles can be assumed to follow the same physical process than in the  
237 atmosphere, although the temperatures can vary over a broad range.

238 The final aerosol flux was directed simultaneously to a condensation particle counter (CPC,  
239 either TSI 3781 or MSP 1040XP models, inlet flow 0.6 L/min), an aerodynamic particle  
240 spectrometer (APS, TSI 3321, inlet flow 1.0 L/min) and a Fourier-transform infrared spectrometer  
241 (Nicolet Magna 860), to obtain particle number, size distribution and their infrared extinction  
242 spectra, respectively. Infrared extinction spectra are recorded in the 650-4000  $\text{cm}^{-1}$  range and 4  $\text{cm}^{-1}$   
243 resolution. Infrared radiation from a colimated source (ORIEL 6580) travels lengthways a 1 m long,  
244 50 mm diameter pyrex absorption cell at ambient temperature with ZnSe windows. The outgoing  
245 radiation is directed to the infrared spectrometer (Figure 1), where the infrared beam is divided into  
246 two. Both beams take slightly different path lengths, and recombine to construct an interferogram.  
247 The recombined intensity is recorded as the path length difference is changed. By applying the  
248 Fourier transform technique, the variation of the intensity with wavenumber is retrieved. The  
249 optical path is sealed and flushed by a current of dry air to reduce interference from ambient water  
250 and carbon dioxide. Background spectra are recorded after pumping out the aerosol cell. Sample  
251 spectra are averaged by collecting typically 32 scans. To complete analytical on-line methodology,  
252 particle shape and size of both pure and mixed particles were determined off-line using a JEOL  
253 JSM-7000F scanning electron microscope (SEM), equipped with a Schottky field emission gun



254 (FEG) and an Oxford Inca Pentafet X3 energy dispersive X-ray analyser (EDX). The EDX  
255 microanalysis was performed using an accelerating voltage of 20 kV and a current intensity of  $10^{-10}$   
256 A, with a working distance of 10 mm. The aerosol of interest was collected at the exit of the  
257 extinction flow cell onto a glass slide, and particles were coated with an Au layer (20 nm) deposited  
258 by evaporation using a Quorum Q150T Sputter Coater to provide electrical conductivity.

259 Particle size distribution in the 0.5-20  $\mu\text{m}$  is retrieved by an aerodynamic particle  
260 spectrometer (TSI 3321), that give a tail in the 0.5-3.5  $\mu\text{m}$  range. Information about the size  
261 distribution of pure salt particles in the 0-0.5  $\mu\text{m}$  range was obtained by processing the SEM images  
262 with the help of the ImageJ software [rsbweb.nih.gov/ij/]. The obtained distribution fitted  
263 satisfactorily to a lognormal distribution with a count median diameter of 46 nm and  $\sigma = 2.0$ .  
264 Particles appear mostly isolated, without a tendency to aggregate. Representative examples of  
265 number size distributions of pure NaCl particles and also covered with hexanoic acid are presented  
266 in Figure 2.

267

268

### 269 **3. RESULTS AND DISCUSSION**

270

#### 271 **3.1. Infrared spectra of pure carboxylic acids**

272

273 The infrared absorption spectra of bulk HA, OA and LA recorded at ambient temperature  
274 are presented in Figure 3. The spectra of HA and OA were recorded in an infrared cell for liquids,  
275 whereas for LA one drop of the sample dissolved in ethanol was deposited on a  $\text{BaF}_2$  window until  
276 solvent evaporation, after which the absorption spectrum of the film was recorded. The main  
277 absorption bands are common to all three acids, with small differences in band position and  
278 intensity.

279 The sharp carbonyl stretching band can be seen near  $1710\text{ cm}^{-1}$ , the broad band in the 2500-  
280  $3500\text{ cm}^{-1}$  range has been assigned to associated  $\text{COO-H}$  stretchings (broadened by intermolecular  
281 association by hydrogen bonding), whereas the group of three peaks in the  $2800\text{-}3000\text{ cm}^{-1}$  range,  
282 exhibiting a different resolvable structure for the different acids, has been assigned to  $\text{-C-H}$   
283 stretchings. A more complex band system appears in the  $800\text{-}1500\text{ cm}^{-1}$ , specific of each acid. On

284 the other hand, the gas phase infrared spectra of the three acids (NIST Chemistry Webbook:  
285 <http://webbook.nist.gov/chemistry>, not shown in Figure 1) show several differences with the bulk  
286 phase spectrum: the intense C=O band locates in the 1780-1790  $\text{cm}^{-1}$ , whereas a narrow band  
287 appears near 3580  $\text{cm}^{-1}$  (COO-H free stretch), absent in the condensed phase. Overlapped bands  
288 appearing in the 2800-3000  $\text{cm}^{-1}$  range are coincident with peak positions in bulk phase spectra.  
289 Finally, a number of bands is present in the 800-1600  $\text{cm}^{-1}$  region, several of which can be  
290 distinguished from condensed phase spectra.

291 Figure 3 also shows the extinction spectra of homogeneously nucleated particles. Bands  
292 belonging to each acid were detected in all cases, their absorption intensity growing with increasing  
293  $T_1$  and  $T_2$ . CPC measurements confirmed the presence of particles, that were assumed to belong to  
294 the carboxylic acids. For HA, the obtained spectra are mostly coincident with the gas phase  
295 spectrum. A weak band located at near 1730  $\text{cm}^{-1}$  has been assigned to the C=O stretch originating  
296 from small particles of liquid HA due to homogeneous nucleation. This band is 21  $\text{cm}^{-1}$  displaced to  
297 higher wavenumbers with respect to bulk liquid HA, possibly due to surface effects in small  
298 particles: due to the interactions between surface molecules and the surrounding medium, the  
299 surface region has different structural properties (and thus spectroscopic features) than the core of  
300 the particles (Firanescu et al 2006). This hypothesis is supported by the spectrum of liquid HA  
301 adsorbed at the air/water interface by vibrational sum-frequency spectroscopy (Soule et al 2007),  
302 that locates the C=O band in the 1726-1730  $\text{cm}^{-1}$  range, depending on the polarization conditions.  
303 For OA, the C=O band was peaked at near 1700  $\text{cm}^{-1}$ , but broader than the one corresponding to  
304 condensed phase. Also an overlapping band system in the 1540-1650  $\text{cm}^{-1}$  range was observed. No  
305 lines of gaseous OA were detected. For LA, no gas band features were present, in accordance with  
306 its low vapor pressure. Further evidence of the presence of particles is given by the baseline  
307 increase to higher wavenumbers (Figure 2), which is indicative of particle scattering (Hinds 1998).  
308 This effect is more pronounced as  $T_2$  is increased. A broad band in the 3100-3500  $\text{cm}^{-1}$  range is  
309 observed for homogeneously nucleated hexanoic and octanoic acid, that is absent in the bulk  
310 spectrum. This feature has been attributed to the presence of small amounts of liquid water  
311 outgassed from the acid that become trapped into the particles.

312 The most notable differences in band wavenumber and bandwidth for the three acids are  
313 observed for the C=O stretching band, and are summarised in Table 2. These differences can be  
314 significant, as can be related with surface effects that can give information about the particles.  
315 Carbonyl bandwidth in the bulk acids is in the 20-29  $\text{cm}^{-1}$  range, and increases with molecular mass.  
316 These values change in homogeneously nucleated organic particles, either increasing (HA and OA)  
317 or decreasing (LA). Relative variations in its magnitude are in the 25-75% range.

318

319

### 320 **3.2. Infrared extinction spectra of heterogeneously nucleated NaX particles with carboxylic** 321 **acids**

322

323 Representative infrared extinction spectra of heterogeneously nucleated sodium halide  
324 particles are shown in Figure 2. The band intensities of heterogeneous nucleation spectra are much  
325 bigger than those of homogeneous nucleation (e.g., 4:1 for NaCl/OA at  $T_1=90^\circ\text{C}$ ,  $T_2=80^\circ\text{C}$ ). For  
326 NaX/HA particles, bands of gaseous and condensed phase HA were observed. The latter increase in  
327 intensity with  $T_1$  and  $T_2$ , whereas the former remain constant. For NaX covered with OA or LA,  
328 practically all infrared bands originate from condensed phase, gas phase OA bands being very weak  
329 or absent. Their observed carbonyl absorption band wavenumber and bandwidth for the various  
330 acids are collected in Table 2. The changes in these magnitudes with respect to their bulk phase  
331 values are indicative of organic molecule/inorganic ion interactions, and can be used to address the  
332 effect of the ionic salt environment near the organic acid molecules. For all acids, the C=O stretch  
333 wavenumber of the acid coating on NaX varies with the salt and is between the wavenumber of the  
334 corresponding bulk acid and that of homogeneously nucleated acid particles (Table 2). In all cases,  
335 bulk wavenumber of C=O locates around  $70\text{ cm}^{-1}$  lower than in the gas phase, bulk LA showing the  
336 lowest wavenumber ( $1700\text{ cm}^{-1}$ ). On the other hand, the bandwidths of the C=O stretch coming  
337 from heterogeneously nucleated particles depend on the nature of the salt, the organic acid and the  
338 degree of covering: for HA-covered particles, the full width half-maximum (FWHM) can reach  $40$   
339  $\text{cm}^{-1}$ , doubling the bulk HA value, whereas for LA-coated particles it is smaller than the bulk acid  
340 bandwidth. The relationship of these results with the hygroscopic properties of particles will be  
341 discussed later.

342

343

### 344 **3.3. Morphology of pure and mixed particles**

345

346 SEM images of pure NaCl and LA particles, and of NaCl particles after covering them with  
347 LA, were recorded and are presented in Figure 4. This technique was not well suited to study

348 particles that included OA or HA, due to their high vapor pressure at room temperature that  
349 diffculted their manipulation in the SEM vacuum chamber. Images of pure NaCl particles show  
350 particles of cubic form as expected but whith their edges somewhat rounded, as a result of a short  
351 exposure of deposited particles to ambient air before being coated with the gold layer; as NaCl is  
352 very hygroscopic, they have uptaken a small amount of gaseous water enough to change their  
353 original morphology (see Figure 4a).

354 Images of LA particles (Figure 4b) show a much smaller amount of particles that tend to  
355 form big aggregates, typically of 1-2  $\mu\text{m}$  length, in accordance with previous studies (Gadermann et  
356 al 2008). The particles are amorphous and mostly elongated. Images of NaCl particles deposited  
357 jointly with LA (after heterogeneous nucleation, see Figure 3c) show a small number of particles,  
358 much fewer than in the case of pure NaCl, although the initial amount of NaCl aerosol was identical  
359 in both cases (this may be due to the low affinity of the mixture with the supporting material or to  
360 higher tube losses). Most particles present cubic form, and tend to appear as aggregates. Although  
361 pure LA particles can be observed, they are very scarce. A thin layer covering the NaCl particles  
362 can be observed, smaller NaCl particles appearing with a thicker covering. Thus it can be said that a  
363 thin layer of lauric acid is deposited on NaCl particles, acting as a glue that tends to link individual  
364 NaCl particles.

365

366

### 367 **3.4. Deliquescence and efflorescence of heterogeneously nucleated NaX particles with HA, OA** 368 **and LA**

369

#### 370 *3.4.1. Infrared spectra of particles at various RHs*

371 To examine the deliquescence behavior, dry NaX particles coated with each of the  
372 carboxylic acids were mixed with a flow of gaseous water at different RHs. As a representative  
373 example, Figure 5 shows three spectra of NaBr particles covered with OA at various RHs. The  
374 presence of liquid water can be detected and quantified by the broad band centered at near  $3400\text{ cm}^{-1}$   
375 <sup>1</sup>. For all cases, no infrared absorption bands arising from aqueous dissolved acids were detected, so  
376 in all the subsequent discussion all the organic acids are assumed to be undissolved in liquid water.

377

378 In all cases, we paid special attention to the C=O stretching band of the acids near 1700 cm<sup>-1</sup>,  
379 and we analyzed it as a function of RH, organic acid and halide anion measured. In OA/NaX and  
380 LA/NaX particles, the carbonyl band absorption intensity of condensed phase acid keeps constant  
381 with RH; on the contrary, for NaX/HA particles the band intensities of liquid HA decrease as RH  
382 increases, although the intensities of gaseous HA remain unchanged. As an example, Figure 6 plots  
383 the intensity variation of the carbonyl band versus RH for liquid and gaseous HA in NaBr particles.  
384 It can be seen that, while the C=O band intensity of gaseous HA keeps roughly constant with RH,  
385 the band intensity for condensed HA lowers at higher RH. The largest decrease was observed in  
386 NaBr, and the smallest in NaI. In all salts, the particles retained liquid HA at RHs higher than their  
387 DRH. On the other hand, the spectrum baseline also decreases at high wavenumber as RH increases  
388 (due to decrease of particle scattering), indicating a thinner coating of the particles.

389 The efflorescence behavior of coated aqueous NaX particles was investigated by passing  
390 NaX aqueous particles along the heated oven containing the carboxylic acid vapor. For all the  
391 systems, at RH near saturation the spectra show bands of condensed phase organic acid. The  
392 intensity of these bands keeps roughly constant with RH in OA and LA, but liquid HA band  
393 intensities decrease notably as RH is reduced (a factor in the range 3-7 from RH≈100% to 27%,  
394 depending on the salt). Figure 5 shows the case for NaBr/HA. Also the scattering signal is  
395 decreased with RH, indicating that particles get smaller.

396

### 397 3.4.2. *Deliquescence and efflorescence curves*

398 Deliquescence and efflorescence curves were recorded by measuring the integrated  
399 absorbance of liquid water in the particles in the 3400-3600 cm<sup>-1</sup> range and plotting the values  
400 versus RH. This interval was selected as it is mostly free of interference with nearby absorption  
401 spectral features. The scattering component of the liquid water extinction spectrum was removed by  
402 subtracting the sloping baseline present at high wavenumbers to obtain integrated absorbances. The  
403 results for all the systems are presented in Figure 6. The curves for the pure inorganic salts have  
404 also been measured and are included in the figure. Hereafter, we describe the effect of the various  
405 acids in each of the inorganic salts.

406

407 1) NaCl particles

408 The deliquescence curve of NaCl/HA is very similar to that of pure NaCl particles, that  
409 deliquesce at DRH (298 K) = 75.3% (Tang and Munkelwitz 1993). No water uptake is detected  
410 until near 73% RH, where particles abruptly become liquid. However, SEM results show that  
411 particles uptake small amounts of water before sudden deliquescence, that are not enough to change  
412 their size, but modify their size slightly (becoming more "roundish" with increasing RH). The  
413 quantity of liquid water uptaken by NaCl particles is unaffected by the presence of the HA  
414 covering. However, for NaCl/OA and NaCl/LA, particle deliquescence occurs near to 56% RH,  
415 substantially lower than in pure NaCl. These results are in agreement with previous reports in which  
416 a slight lowering of the DRH of NaCl was observed when the particles were covered with OA and  
417 LA acids (Hansson et al 1998). In NaCl/OA, the particles uptake larger amounts of water vapour  
418 than in pure NaCl, whereas the opposite is observed for NaCl/LA. The efflorescence curves for all  
419 the three acids locate the ERH close to 40%, very similar to pure NaCl particles. The curves are  
420 coincident in the RH=20-60% range, but diverge towards higher RHs. For all acids, particles retain  
421 larger amounts of water than pure NaCl in the RH=60-95%, the quantities being in the order  
422 LA>OA>HA. Also the amount of HA and OA in the particles decreases as liquid water is removed  
423 from them until the ERH is reached, whereas no change in the amount of LA is observed with RH.

424

## 425 2) NaBr particles

426 According to Figure 7 data, NaBr/HA particles deliquesce at somewhat higher RH than pure  
427 NaBr particles: liquid water in NaBr/HA particles is not detected until 49.6% RH. This value does  
428 not change with the degree of coating, and contrasts with the value of DRH=37% for pure NaBr  
429 particles (Minambres et al 2008). On the other hand, OA and LA coverings do not have any effect  
430 on the deliquescence behavior of NaBr: the deliquescence curves are practically coincident with  
431 those of pure NaBr. Also, the amount of uptaken water is similar to pure NaBr, except for OA-  
432 covered particles, that grow faster for RH>70%. Efflorescence curves for all acid covering are very  
433 similar to pure NaBr (ERH=23%) in the 20-60% RH (although OA retains slightly more water at all  
434 RHs), but at RH>60% acid-covered particles retain higher amounts of liquid water than pure NaBr  
435 (up to double for NaBr/LA at 90% RH). Thus the presence of the organic covering causes water  
436 loss to happen more gradually than in the pure salt at high RHs.

437

## 438 3) NaI particles

439 The deliquescence curves of acid-covered NaI particles exhibit substantial differences with  
440 respect to the pure salt. Whereas pure NaI particles take up water at all RHs (Minambres et al  
441 2011), NaI/HA and NaI/LA particles do not uptake water until RH=16% and 21%, respectively.  
442 Liquid water is not detected in NaI/OA particles until RH=75%. It can be concluded that organic  
443 acid covering substantially retards the uptake of water in NaI particles, specially OA. The amount  
444 of liquid water in HA and LA-covered particles in the RH=20-80% is higher than in pure NaI. The  
445 efflorescence curve of NaI/LA is practically coincident with the pure NaI curve in the RH range  
446 measured. However, HA-covered particles lose water more gradually, retaining higher amounts of  
447 water than pure NaI in the RH=30-80% range. Finally, OA-covered particles follow closely the  
448 pure salt curve for RH>80%, but retain more water at lower RHs. The general tendency is that the  
449 presence of acid covering retains more water in the particles, except for LA, which shows little  
450 effect.

451

#### 452 3.4.3. *Discussion of deliquescence and efflorescence processes*

453 The obtained results on the hygroscopicity of sodium halide particles covered with organic  
454 acids having low water solubility show an overall complex behavior. The deliquescence curves of  
455 Fig. 7 indicate that the water uptake process is dependent on both the inorganic salt and the organic  
456 acid. Whereas HA, OA and LA have a smaller effect on water uptake of NaBr (only HA slightly  
457 retards the DRH), they produce a lowering of the DRH in NaCl respect to the pure salt. On the  
458 contrary, in NaI these acids prevent particles to uptake liquid water at low RHs, unlike in pure NaI,  
459 which admits water at any RH. This retarding effect is especially attributed to OA. In efflorescence,  
460 a similar behavior is observed for all systems: the presence of the organic acid makes the particle to  
461 retain more water at a given RH, all curves converging at the ERH.

462 The observed hygroscopic behavior can be due to several factors. Although the morphology  
463 of particles can sometimes influence their hygroscopic behavior, all NaX salt dry particles are  
464 expected to be cubic, as all of them have an octahedral crystal structure. Another possibility is that  
465 each organic acid interacts differently with each inorganic salt. Organic acids in the surface of  
466 inorganic salts will tend to orientate with their polar groups facing the salt surface, so that ion-  
467 dipole interactions will arise that will diminish the system Gibbs free energy. The polarizability of  
468 the halogen atoms increases in the order Cl (14.7) < Br (21.8) < I (35.1, all in atomic units) (P.  
469 Schwerdtfeger, Table of experimental and calculated static dipole polarizabilities for the electronic  
470 ground states of the neutral elements, <http://ctcp.massey.ac.nz/dipole-polarizabilities>), so  
471 differences in the interaction magnitude are expected. In addition, the surface of particles will

472 become more populated by anions as halide polarizability increases (Jungwirth and Tobias 2001).  
473 Also elongated carbonated chains are known to be easily polarizable. Additionally, it has been  
474 proposed that the structure of the monolayers formed with insoluble surfactants determines their  
475 resistance towards gas uptake (Stemmler et al 2008). Fatty acids form a highly ordered film in the  
476 so-called liquid condensed state, whereas in the liquid expanded state they form a less ordered film  
477 and do not hinder the uptake. In that way, the differences in retardation in water uptake can arise  
478 from the different degrees of compression of such films (Donaldson and Vaida 2006; Takahama and  
479 Russell 2011). Another possibility is that gaseous water transport occurs through open sections of  
480 the surface, that can be due to incomplete packing by the organic film or to random fluctuations  
481 (Donaldson and Vaida 2006). The observed salt-specific behavior is in accordance with the  
482 observed deliquescent behavior of internally mixed particles formed of sodium halide and water  
483 soluble organic acids (Minambres et al 2011).

484 The hygroscopic behavior can be correlated with the spectral features of the organic acids  
485 shown in Table 2, where the wavenumber and the bandwidth of the C=O band in different  
486 environments are shown. The band center wavenumbers shift in the  $-6 / +10 \text{ cm}^{-1}$  range in the  
487 presence of NaX salts, but the bandwidth (FWHM) variation (respect to the C=O vibration for the  
488 bulk acid) is in the  $-16 / +20 \text{ cm}^{-1}$  range, representing a change in the FWHM of more than 100% in  
489 some cases. The wavenumber shift and broadening of a spectral band may arise from a change in  
490 the internal force constant of the C=O bond due to the formation of intermolecular bonds with other  
491 molecules, for example hydrogen bonds with water (Kalsi 2007). These results are indicative of the  
492 effect of the ionic salt environment near organic acid molecules. Although it is not easy to establish  
493 clear correlations with the changes in deliquescence behavior, some remarks can be outlined. For  
494 systems with NaBr, the changes in the FWHM of the C=O band are the smallest (except for  
495 HA/NaBr), which correlate with a quite small change of DRH (except for HA/NaBr). For NaI  
496 mixed with an organic acid, although the changes in FWHM are considerable (indicating strong  
497 ion-polar head group interaction), the explanation for the water uptake behavior can be attributed to  
498 the hydrophobic effect exerted by the organic acids, forming a barrier that prevents the entrance of  
499 gaseous water molecules inside the particles. This effect is very pronounced for NaI/OA, and we  
500 have not found a satisfactory explanation for it. Finally, in NaCl/organic acid systems, the opposite  
501 effect is observed, in which the presence of acids slightly enhance the entrance of gaseous water.  
502 This can be attributed to the ion-polar group interaction that slightly lowers the Gibbs free energy of  
503 the system, favoring the acceptance of gaseous water molecules. The efflorescence process in NaX  
504 aqueous particles is not substantially affected by the presence of the acid. As there is not an energy  
505 barrier to the efflorescence process (in contrast to deliquescence), water loss takes place gradually



506 as RH is lowered. Additionally, the salting out effect of NaCl will make dissolved organic acid  
507 molecules (specially the most water soluble HA) gradually move to the surface as the concentration  
508 of the salt solution increases (Demou and Donaldson 2002), and will be eventually removed from  
509 the surface together with water. However, the magnitude of the salting out effect for HA is rather  
510 small (Demou and Donaldson 2002).

511 The results on water uptake and release in the special case of HA covered particles give  
512 information on how the dynamics of water exchange in inorganic particles is affected by the  
513 presence of a surface layer having small water solubility. In all deliquescence curves, there is a  
514 competition for surface positions between adsorbed HA and gaseous water, as indicated by the  
515 evolution of the amounts of liquid HA and water with RH (or, equivalently, the relative amount of  
516 gaseous water) in Figure 6. This can be reasoned as follows: in the deliquescence spectrum of  
517 Figure 6, the amount of liquid HA decreases as RH (and consequently the amount of gaseous water)  
518 increases, indicating that, if we start from a dry crystalline NaX particle covered with HA, gaseous  
519 water tends to displace HA molecules away from the particle surface, to try to accommodate  
520 themselves on the NaX solid surface. This effect must be a consequence of the change in the Gibbs  
521 free energy of the system in the deliquescence process: as the energetically most stable system is  
522 obtained when gaseous water molecules remain near the solid NaX surface (producing  
523 deliquescence when the number of gaseous water molecules reaches a given value), HA molecules  
524 will tend to be displaced from their surface locations. In efflorescence, however, the observed  
525 behavior is different: removal of liquid water from aqueous particles having an organic HA coating  
526 due to the decrease of RH is accompanied by removal of HA from the particle surface. This effect  
527 can be explained assuming that liquid HA uniformly covers the NaX aqueous particle. For water  
528 molecules to exit the particles, a "hole" in the HA layer must be made, and water molecules exiting  
529 the particle will sweep away HA molecules from their surface locations. NaX-gaseous water  
530 interactions must be stronger in NaCl than in NaBr and NaI or, alternatively, NaX-HA interactions  
531 will be weaker for NaCl than for NaBr and NaI. For that reason, in NaX/HA particles, HA is  
532 displaced more effectively from the surface at the DRH of pure NaCl. In NaBr and NaI, however,  
533 the number density of gaseous water molecules nearby the particles at the DRH of the pure  
534 inorganic particle is not enough to remove the HA cover, and a higher number of gaseous water  
535 molecules (higher RH) is needed to produce particle deliquescence.

536

537

538 **3.5. Estimation of the relative amounts of organic acid and water in the particles**

540 The relative amounts of liquid water and a given organic acid in the aqueous NaX particles  
 541 can be calculated on average from measured absorbances in their infrared spectra. The number of  
 542 molecules  $N_i$  of a given species  $i$  per unit volume of aerosol sample is related with the integrated  
 543 band absorbance of that species via the Beer-Lambert law (Weis and Ewing 1996):  
 544  $\bar{A}_i = \bar{\sigma}_i N_i z / 2.303 \times 10^2$ , where  $\bar{A}_i$  is the integrated absorbance of a given band ( $\text{cm}^{-1}$ ),  $\bar{\sigma}_i$  the  
 545 integrated absorption cross section per molecule ( $\text{m molecule}^{-1}$ ) of that band, and  $z$  is the optical  
 546 path length of the aerosol flow cell (m). Applying the previous equation, we can obtain the organic  
 547 acid/liquid water mole ratio for samples measured in the same aerosol cell, if  $\bar{A}_i$  and  $\bar{\sigma}_i$  are known:  
 548  $N_{\text{org}} / N_{\text{H}_2\text{O}} = \bar{A}_{\text{org}} \bar{\sigma}_{\text{H}_2\text{O}} / \bar{A}_{\text{H}_2\text{O}} \bar{\sigma}_{\text{org}}$ . The absorption cross section of liquid water has been obtained  
 549 from pure water data in the 2800-3600  $\text{cm}^{-1}$  range (Downing and Williams 1975),  $\bar{\sigma}_{\text{H}_2\text{O}} = 1.3 \times 10^{-18}$   
 550  $\text{m molecule}^{-1}$ . The absorption cross sections for liquid HA and OA have been obtained by  
 551 measuring the integrated absorbance of a solution of the acid in methanol of known composition in  
 552 a 150  $\mu\text{m}$  long cell for liquid samples. The C=O band in the 1668-1774  $\text{cm}^{-1}$  range was chosen to  
 553 compute the integrated absorbance. The obtained values are  $\bar{\sigma}_{\text{HA}} = 9.87 \times 10^{-19}$   $\text{m molecule}^{-1}$  and  
 554  $\bar{\sigma}_{\text{OA}} = 1.71 \times 10^{-19}$   $\text{m molecule}^{-1}$ . From these data, the average  $N_{\text{HA}}/N_{\text{H}_2\text{O}}$  and  $N_{\text{OA}}/N_{\text{H}_2\text{O}}$  ratios have  
 555 been calculated for the various salts at several RHs. The results appear in Figure 8. The obtained  
 556 results indicate that  $N_{\text{HA}}/N_{\text{H}_2\text{O}}$  values are comprised in the 0.1-0.6 range for RH in the 30-98%  
 557 interval, the lowest values corresponding to the highest RHs. In contrast, the  $N_{\text{OA}}/N_{\text{H}_2\text{O}}$  quotient  
 558 spans from 0.2 to 1.9 (for RHs in the 40-96% range), when again the highest values correspond to  
 559 the lowest RH conditions. The highest  $N_{\text{OA}}/N_{\text{H}_2\text{O}}$  ratio (1.9) is obtained for NaI efflorescing  
 560 particles. The results in Fig. 8 indicate that, in general, OA-covered particles tend to displace liquid  
 561 water more efficiently than HA-covered particles.

562 The spectroscopic results indicate that gaseous HA, OA and LA easily nucleate onto dry and  
 563 aqueous NaX particles. The amount of acid uptaken increases with the temperature of the oven.  
 564 Additionally, SEM images of NaCl particles with LA show NaCl particle aggregates, indicating that  
 565 they are "glued" by lauric acid. However, SEM images provide no visual evidence of the presence  
 566 of an organic cover, so we can conclude that the cover must be much thinner than the size of the salt  
 567 particles. A rough higher limit for the cover thickness can be set at 20 nm, which is the resolution of  
 568 the SEM images. This estimate can be compared with HA and OA cover thickness on aqueous  
 569 particles, calculated assuming that liquid HA or OA arrange in a hydrophobic organic layer in the  
 570 surface of an aqueous particle, according to one proposed model (Ellison et al 1999), and taking

571 into account the spectrally measured relative proportions of water and organic acid. The volume of  
572 a spherical aqueous particle of radius  $R$  will be  $V_{\text{H}_2\text{O}} = (4/3)\pi R^3$ , whereas the volume of liquid  
573 organic coating of thickness  $r$ , assuming uniform coverage, can be written as  $V_{\text{org}} = (4/3)\pi[(R+r)^3 -$   
574  $R^3]$ . On the other hand,  $V_{\text{org}}/V_{\text{H}_2\text{O}} = N_{\text{org}}\rho_{\text{H}_2\text{O}}/(N_{\text{H}_2\text{O}}\rho_{\text{org}})$ , where  $\rho$  stands for density. As the  $N_{\text{org}}/N_{\text{H}_2\text{O}}$   
575 ratios have been determined previously, from the previous equations we can obtain  $r$  in terms of the  
576 aqueous particle radius  $R$ :

$$577 \quad r/R = [1 + N_{\text{org}}\rho_{\text{H}_2\text{O}}/(N_{\text{H}_2\text{O}}\rho_{\text{org}})]^{1/3} - 1$$

578 For typical values of  $N_{\text{HA}}/N_{\text{H}_2\text{O}} = 0.1, 0.3$  and  $0.6$ ,  $r/R = 0.035, 0.098$  and  $0.181$ ,  
579 respectively, indicating that the thickness of the organic layer increases roughly linearly with the  
580 number of molecules of liquid HA. For example, if  $N_{\text{HA}}/N_{\text{H}_2\text{O}} = 0.3$  and  $R = 0.3 \mu\text{m}$  (roughly  
581 corresponding to NaCl particles appearing in Figure 4c), the HA coating thickness yields an  
582 estimation of  $r = 29 \text{ nm}$  for a particle coated with HA. This value can be compared with the upper  
583 limit of  $20 \text{ nm}$  estimated for the cover thickness in the LA/NaCl system. The former HA-coating  
584 thickness is much bigger than the estimated thickness of a monolayer, although we cannot affirm  
585 whether the particles are uniformly covered. Previous investigations indicate that the degree of  
586 insoluble acid coverage do not substantially alter DRH. Complete coverage of inorganic particles by  
587 fatty acids had no dramatic effect on NaCl particle DRH (Andrews and Larson 1993). On the other  
588 hand, DRH of ammonium sulfate was only slightly lowered for oleic acid thickness up to  $109 \text{ nm}$   
589 (Najera and Horn 2009), much bigger than our estimated thickness of around  $30 \text{ nm}$ . No variations  
590 in DRH with acid covering thickness were observed in this work.

591

592

#### 593 **4. CONCLUSIONS AND ATMOSPHERIC IMPLICATIONS**

594

595 This work has studied the effect of a covering layer of hexanoic, octanoic and lauric acid,  
596 which are present in the Earth's troposphere, on the hygroscopic properties of sodium halide  
597 submicrometer particles, which are constituents of sea salt aerosol. Infrared extinction spectroscopy  
598 together with particle counting and visualizing techniques has allowed to detect the formation of  
599 homogeneously and heterogeneously nucleated particles and the variation of their composition in  
600 the presence of variable amounts of gaseous water, leading to the processes of deliquescence and  
601 efflorescence. SEM measurements and data deduced from infrared absorbance spectra indicate that

602 the covering thickness of the obtained salt particles is compatible with an average value of 30 nm.  
603 SEM images show that the effect of lauric acid on NaCl is to agglomerate salt particles, producing  
604 bigger effective particles. It has not been possible to observe this effect with the other acids, due to  
605 experimental inconveniences.

606 It has been found that the hygroscopic properties of sodium halide particles covered with  
607 hexanoic, octanoic or lauric acid change both with the nature of the inorganic salt and the  
608 carboxylic acid. The DRH of NaCl aerosol is dependent on the organic acid covering the particles,  
609 the deliquescence of NaCl/OA and NaCl/LA systems occurring near RH=56%, considerably lower  
610 than in pure NaCl. On the other hand, NaBr covered particles do not substantially alter their water  
611 uptake behavior respect to pure salt particles, irrespective of the organic acid. The growth factor of  
612 these particles is also unaffected by the organic coating. Finally, organic acid covering on solid NaI  
613 particles acts as a barrier to water uptake; NaI pure particles deliquesce at about 15% RH when  
614 coated with hexanoic and lauric acid, but the DRH increases remarkably up to 60% RH for octanoic  
615 acid covered particles. The general consequence is that the water uptake behavior of sodium halide  
616 particles coated with organic acids is dependent on the nature of the anion and the carboxylic acid.  
617 This is in accordance with former studies of sodium halides with succinic acid, which showed a  
618 salt-specific behavior. Consequently, although it is customary to extrapolate the water uptake  
619 behavior of NaCl particles to sea salt aerosol, due to the predominance of this species in marine salt,  
620 the detailed picture can be more complex. Regarding efflorescence process, the obtained results  
621 indicate that the overall effect of the organic acid cover is to retain higher amounts of water at RH  
622 in the 60-90% range with respect to pure NaX particles. In NaCl particles the longer chain acid  
623 (LA) achieves the highest water retention, while the shortest one (HA) achieves the lowest. All  
624 acids act similarly in NaBr aqueous particles, whereas in aqueous NaI particles OA is the acid that  
625 produces higher water retention at RH in the 60-90% range. The results show that this barrier effect  
626 is dependent on the nature of the organic acid, and can have important consequences for the  
627 troposphere, as the organic species can determine the amount of liquid water in the particles and  
628 their phase at a given RH. Finally, the measurements indicate that there is no simple correlation  
629 between water uptake of crystallization processes in coated salt particles and the length of the  
630 carbonated chain in the carboxylic acid. The complex behavior in hygroscopic properties in the  
631 different salts can not be easily attributed to a single effect, and the results point to more specific  
632 ion-molecule interactions in the NaX/organic acid/H<sub>2</sub>O systems or to the structure of the organic  
633 film on the particle.

634 Several consequences for the atmosphere can be driven from this study: as bromine and  
635 iodine ions tend to segregate to the surface of marine aerosol particles, and the effect of fatty acids

636 on them can be different as compared to the more abundant NaCl species, this may influence the  
637 surface properties of the particles not usually taken into account in the models. At a given value of  
638 ambient relative humidity, sea salt particles may have an outer core in which NaBr and NaI are  
639 more abundant, and if an organic layer having low water solubility is present, the interactions of the  
640 organic compound will predominantly take place with bromide and iodide ions. At given conditions  
641 of relative humidity in the atmosphere, liquid water amounts and phase of sea-salt particle outer  
642 core may vary regard to the expected behavior of pure NaCl particles. This has consequences in the  
643 heterogeneous processes taking place between particles and atmospheric gases, such as gas uptake  
644 and chemical reactivity.

645

646

647

#### **ACKNOWLEDGMENTS**

648

649

650

651

652

653

654

655

The authors are grateful to Ministerio de Ciencia e Innovación (Madrid) for grant-in-aids (CGL2011-22441 and Consolider CSD-2007-00013), to Gobierno Vasco/Eusko Jaurlaritza (Vitoria-Gasteiz) for a Consolidated Research Group grant (IT520-10), and UPV/EHU for UFI11/23, SEM facilities (SGI/IZO-SGIker) and general support. L.M. thanks UPV/EHU for a postdoctoral research grant. We are grateful to Dr. Cristina Gutiérrez from UPV/EHU for the use of the butanol CPC.

656 **REFERENCES**

657

- 658 Abbatt, J., Broekhuizen, K., and Pradeep Kumar, P. 2005. Cloud condensation nucleus activity of  
659 internally mixed ammonium sulfate/organic acid aerosol particles. *Atmos.Environ.* 39:4767-4778.
- 660 Andreae, M., and Rosenfeld, D. 2008. Aerosol–cloud–precipitation interactions. Part 1. The nature  
661 and sources of cloud-active aerosols. *Earth-Sci.Rev.* 89:13-41.
- 662 Andrews, E., and Larson, S. M. 1993. Effect of Surfactant Layers on the Size Changes of Aerosol-  
663 Particles as a Function of Relative-Humidity. *Environ.Sci.Technol.* 27.
- 664 Ault, A. P., Moffet, R. C., Baltusaitis, J., Collins, D. B., Ruppel, M. J., Cuadra-Rodriguez, L. A.,  
665 Zhao, D., Guasco, T. L., Ebben, C. J., and Geiger, F. M. 2013. Size-dependent changes in sea spray  
666 aerosol composition and properties with different seawater conditions. *Environ.Sci.Technol.*  
667 47:5603-5612.
- 668 Baker, A. R. 2005. Marine aerosol iodine chemistry: The importance of soluble organic iodine.  
669 *Environmental Chemistry.* 2.
- 670 Bialek, J., Dall'Osto, M., Monahan, C., Beddows, D., and O'Dowd, C. 2012. On the contribution of  
671 organics to the North East Atlantic aerosol number concentration. *Environmental Research Letters.*  
672 7:044013.
- 673 Carpenter, L. J. 2003. Iodine in the marine boundary layer. *Chem.Rev.* 103:4953-4962.
- 674 Carslaw, K., Boucher, O., Spracklen, D., Mann, G., Rae, J., Woodward, S., and Kulmala, M. 2010.  
675 A review of natural aerosol interactions and feedbacks within the Earth system. *Atmospheric*  
676 *Chemistry and Physics.* 10:1701-1737.
- 677 Cavalli, F., Facchini, M. C., Decesari, S., Mircea, M., Emblico, L., Fuzzi, S., Ceburnis, D., Yoon,  
678 Y. J., O'Dowd, C. D., Putaud, J. P., and Dell'Acqua, A. 2004. Advances in characterization of size-  
679 resolved organic matter in marine aerosol over the North Atlantic. *Journal of Geophysical*  
680 *Research-Atmospheres.* 109:D24215.
- 681 Chakraborty, P., and Zachariah, M. R. 2008. Sticking coefficient and processing of water vapor on  
682 organic-coated nanoaerosols. *Journal of Physical Chemistry a.* 112.
- 683 Chuang, P. Y. 2003. Measurement of the timescale of hygroscopic growth for atmospheric aerosols.  
684 *Journal of Geophysical Research-Atmospheres.* 108:4282.
- 685 Ciobanu, V. G., Marcolli, C., Krieger, U. K., Weers, U., and Peter, T. 2009. Liquid– liquid phase  
686 separation in mixed organic/inorganic aerosol particles. *The Journal of Physical Chemistry A.*  
687 113:10966-10978.
- 688 Cwiertny, D. M., Young, M. A., and Grassian, V. H. 2008. Chemistry and Photochemistry of  
689 Mineral Dust Aerosol\*. *Annu.Rev.Phys.Chem.* 59:27-51.
- 690 D O'Dowd, C., and De Leeuw, G. 2007. Marine aerosol production: a review of the current  
691 knowledge. *Philosophical Transactions of the Royal Society A: Mathematical, Physical and*  
692 *Engineering Sciences.* 365:1753-1774.

- 693 Dall'Osto, M., Ceburnis, D., Martucci, G., Bialek, J., Dupuy, R., Jennings, S., Berresheim, H.,  
694 Wenger, J., Healy, R., and Facchini, M. 2010. Aerosol properties associated with air masses  
695 arriving into the North East Atlantic during the 2008 Mace Head EUCAARI intensive observing  
696 period: an overview. *Atmospheric Chemistry & Physics*. 10.
- 697 Davies, J. F., Miles, R. E., Haddrell, A. E., and Reid, J. P. 2013. Influence of organic films on the  
698 evaporation and condensation of water in aerosol. *Proceedings of the National Academy of  
699 Sciences*. 110:8807-8812.
- 700 Demou, E., and Donaldson, D. J. 2002. Adsorption of atmospheric gases at the air-water interface.  
701 4: The influence of salts. *Journal of Physical Chemistry a*. 106.
- 702 Dennis-Smith, B. J., Hanford, K. L., Kwamena, N. A., Miles, R. E. H., and Reid, J. P. 2012.  
703 Phase, Morphology, and Hygroscopicity of Mixed Oleic Acid/Sodium Chloride/Water Aerosol  
704 Particles before and after Ozonolysis. *Journal of Physical Chemistry a*. 116.
- 705 Donaldson, D. J., and Vaida, V. 2006. The influence of organic films at the air-aqueous boundary  
706 on atmospheric processes. *Chem.Rev.* 106.
- 707 Downing, H. D., and Williams, D. 1975. Optical constants of water in the infrared. *Journal of  
708 Geophysical Research*. 80:1656-1661.
- 709 Duce, R., Mohnen, V., Zimmerman, P., Grosjean, D., Cautreels, W., Chatfield, R., Jaenicke, R.,  
710 Ogren, J., Pellizzari, E., and Wallace, G. 1983. Organic material in the global troposphere.  
711 *Rev.Geophys.* 21:921-952.
- 712 Ebben, C. J., Ault, A. P., Ruppel, M. J., Ryder, O. S., Bertram, T. H., Grassian, V. H., Prather, K.  
713 A., and Geiger, F. M. 2013. Size-Resolved Sea Spray Aerosol Particles Studied by Vibrational Sum  
714 Frequency Generation. *The Journal of Physical Chemistry A*. 117:6589-6601.
- 715 Ellison, G. B., Tuck, A. F., and Vaida, V. 1999. Atmospheric processing of organic aerosols.  
716 *Journal of Geophysical Research-Atmospheres*. 104.
- 717 Fierz-Schmidhauser, R., Zieger, P., Vaishya, A., Monahan, C., Bialek, J., O'Dowd, C., Jennings, S.,  
718 Baltensperger, U., and Weingartner, E. 2010. Light scattering enhancement factors in the marine  
719 boundary layer (Mace Head, Ireland). *Journal of Geophysical Research: Atmospheres (1984–2012)*.  
720 115.
- 721 Finlayson-Pitts, B. J. 2009. Reactions at surfaces in the atmosphere: integration of experiments and  
722 theory as necessary (but not necessarily sufficient) for predicting the physical chemistry of aerosols.  
723 *Physical Chemistry Chemical Physics*. 11:7760-7779.
- 724 Finlayson-Pitts, B. 2003. The tropospheric chemistry of sea salt: A molecular-level view of the  
725 chemistry of NaCl and NaBr. *Chem.Rev.* 103:4801-4822.
- 726 Firanescu, G., Hermsdorf, D., Ueberschaer, R., and Signorell, R. 2006. Large molecular aggregates:  
727 From atmospheric aerosols to drug nanoparticles. *Physical Chemistry Chemical Physics*. 8:4149-  
728 4165.
- 729 Freney, E. J., Martin, S. T., and Buseck, P. R. 2009. Deliquescence and efflorescence of potassium  
730 salts relevant to biomass-burning aerosol particles. *Aerosol Science and Technology*. 43:799-807.

- 731 Frinak, E. K., and Abbatt, J. P. D. 2006. Br(2) production from the heterogeneous reaction of gas-  
732 phase OH with aqueous salt solutions: Impacts of acidity, halide concentration, and organic  
733 surfactants. *Journal of Physical Chemistry a*. 110.
- 734 Gadermann, M., Preston, T. C., Troster, C., and Signorell, R. 2008. Characterization of palmitic and  
735 lauric acid aerosols from rapid expansion of supercritical CO<sub>2</sub> solutions. *Mol.Phys.* 106:945-953.
- 736 Gantt, B., and Meskhidze, N. 2013. The physical and chemical characteristics of marine primary  
737 organic aerosol: a review. *Atmospheric Chemistry and Physics*. 13:3979-3996.
- 738 Garland, E. R., Rosen, E. P., Clarke, L. I., and Baer, T. 2008. Structure of submonolayer oleic acid  
739 coverages on inorganic aerosol particles: evidence of island formation. *Physical Chemistry  
740 Chemical Physics*. 10.
- 741 Garland, R. M., Wise, M. E., Beaver, M. R., DeWitt, H. L., Aiken, A. C., Jimenez, J. L., and  
742 Tolbert, M. A. 2005. Impact of palmitic acid coating on the water uptake and loss of ammonium  
743 sulfate particles. *Atmospheric Chemistry and Physics*. 5:1951-1961.
- 744 Ghosal, S., Brown, M. A., Bluhm, H., Krisch, M. J., Salmeron, M., Jungwirth, P., and Hemminger,  
745 J. C. 2008. Ion Partitioning at the Liquid/Vapor Interface of a Multicomponent Alkali Halide  
746 Solution: A Model for Aqueous Sea Salt Aerosols. *Journal of Physical Chemistry a*. 112.
- 747 Gill, P., Graedel, T., and Weschler, C. 1983. Organic films on atmospheric aerosol particles, fog  
748 droplets, cloud droplets, raindrops, and snowflakes. *Rev.Geophys.* 21:903-920.
- 749 Hämeri, K., Rood, M., and Hansson, H. 1992. Hygroscopic properties of a NaCl aerosol coated with  
750 organic compounds. *J.Aerosol Sci.* 23:437-440.
- 751 Hansson, H. C., Rood, M. J., Koloutsou-Vakakis, S., Hameri, K., Orsini, D., and Wiedensohler, A.  
752 1998. NaCl aerosol particle hygroscopicity dependence on mixing with organic compounds.  
753 *J.Atmos.Chem.* 31.
- 754 Hayase, S., Yabushita, A., Kawasaki, M., Enami, S., Hoffmann, M. R., and Colussi, A. J. 2011.  
755 Weak Acids Enhance Halogen Activation on Atmospheric Water's Surfaces. *Journal of Physical  
756 Chemistry a*. 115.
- 757 Hinds, W. C. 1998. *Aerosol technology :properties, behavior, and measurement of airborne  
758 particles*. John Wiley & Sons.
- 759 Hunt, S. W., Roeselova, M., Wang, W., Wingen, L. M., Knipping, E. M., Tobias, D. J., Dabdub, D.,  
760 and Finlayson-Pitts, B. J. 2004. Formation of molecular bromine from the reaction of ozone with  
761 deliquesced NaBr aerosol: Evidence for interface chemistry. *Journal of Physical Chemistry a*. 108.
- 762 ICCP, 2. 2013. *Clouds and Aerosols*. Pages 571 in: *Climate Change 2013: The Physical Science  
763 Basis*. Contribution of Working Group I to the Fifth Assessment Report of the Intergovernmental  
764 Panel on Climate Change. Anonymous . Cambridge University Press: Cambridge, United Kingdom  
765 and New York, NY, USA.
- 766 Jungwirth, P., and Tobias, D. J. 2001. Molecular structure of salt solutions: a new view of the  
767 interface with implications for heterogeneous atmospheric chemistry. *The Journal of Physical  
768 Chemistry B*. 105:10468-10472.



- 769 Kalsi, P. 2007. Spectroscopy of organic compounds. New Age International.
- 770 Kleefeld, S., Hoffer, A., Krivacsy, Z., and Jennings, S. 2002. Importance of organic and black  
771 carbon in atmospheric aerosols at Mace Head, on the west coast of Ireland (53 19' N, 9 54' W).  
772 Atmos.Environ. 36:4479-4490.
- 773 Krueger, B. J., Grassian, V. H., Iedema, M. J., Cowin, J. P., and Laskin, A. 2003. Probing  
774 heterogeneous chemistry of individual atmospheric particles using scanning electron microscopy  
775 and energy-dispersive X-ray analysis. Anal.Chem. 75:5170-5179.
- 776 Kwamena, N. -. A., Buajarern, J., and Reid, J. P. 2010. Equilibrium Morphology of Mixed  
777 Organic/Inorganic/Aqueous Aerosol Droplets: Investigating the Effect of Relative Humidity and  
778 Surfactants. Journal of Physical Chemistry a. 114.
- 779 Lewis, R., and Schwartz, E. 2004. Sea salt aerosol production: mechanisms, methods,  
780 measurements and models—a critical review. American Geophysical Union.
- 781 Lide, D. R. 1994. CRC handbook of chemistry and physics. CRC press: Boca Raton, FL.
- 782 Limbeck, A., and Puxbaum, H. 1999. Organic acids in continental background aerosols.  
783 Atmos.Environ. 33:1847-1852.
- 784 Ma, X., Chakraborty, P., Henz, B. J., and Zachariah, M. R. 2011. Molecular dynamic simulation of  
785 dicarboxylic acid coated aqueous aerosol: structure and processing of water vapor. Physical  
786 Chemistry Chemical Physics. 13:9374-9384.
- 787 Martin, S. T. 2000. Phase transitions of aqueous atmospheric particles. Chem.Rev. 100:3403-3453.
- 788 Metzger, S., and Lelieveld, J. 2007. Reformulating atmospheric aerosol thermodynamics and  
789 hygroscopic growth into fog, haze and clouds. Atmospheric Chemistry and Physics. 7:3163-3193.
- 790 Middlebrook, A. M., Murphy, D. M., and Thomson, D. S. 1998. Observations of organic material in  
791 individual marine particles at Cape Grim during the First Aerosol Characterization Experiment  
792 (ACE 1). Journal of Geophysical Research. 103:16475-16,483.
- 793 Mikhailov, E., Vlasenko, S., Rose, D., and Pöschl, U. 2013. Mass-based hygroscopicity parameter  
794 interaction model and measurement of atmospheric aerosol water uptake. Atmospheric Chemistry  
795 and Physics. 13:717-740.
- 796 Minambres, L., Mendez, E., Sanchez, M. N., Castano, F., and Basterretxea, F. J. 2011. Water  
797 uptake properties of internally mixed sodium halide and succinic acid particles. Atmos.Environ. 45.
- 798 Minambres, L., Sanchez, M. N., Castano, F., and Basterretxea, F. J. 2010. Hygroscopic Properties  
799 of Internally Mixed Particles of Ammonium Sulfate and Succinic Acid Studied by Infrared  
800 Spectroscopy. Journal of Physical Chemistry a. 114.
- 801 Minambres, L., Sanchez, M. N., Castano, F., and Basterretxea, F. J. 2008. Infrared spectroscopic  
802 properties of sodium bromide aerosols. Journal of Physical Chemistry a. 112.
- 803 Mochida, M., Kitamori, Y., Kawamura, K., Nojiri, Y., and Suzuki, K. 2002. Fatty acids in the  
804 marine atmosphere: Factors governing their concentrations and evaluation of organic films on sea-  
805 salt particles. Journal of Geophysical Research-Atmospheres. 107:4325.

- 806 Najera, J. J., and Horn, A. B. 2009. Infrared spectroscopic study of the effect of oleic acid on the  
807 deliquescence behaviour of ammonium sulfate aerosol particles. *Physical Chemistry Chemical*  
808 *Physics*. 11.
- 809 O'Dowd, C. D., Facchini, M. C., Cavalli, F., Ceburnis, D., Mircea, M., Decesari, S., Fuzzi, S.,  
810 Yoon, Y. J., and Putaud, J. 2004. Biogenically driven organic contribution to marine aerosol.  
811 *Nature*. 431:676-680.
- 812 O'Dowd, C. D., Jimenez, J. L., Bahreini, R., Flagan, R. C., Seinfeld, J. H., Hämeri, K., Pirjola, L.,  
813 Kulmala, M., Jennings, S. G., and Hoffmann, T. 2002. Marine aerosol formation from biogenic  
814 iodine emissions. *Nature*. 417:632-636.
- 815 O'Dowd, C. D., Smith, M. H., Consterdine, I. E., and Lowe, J. A. 1997. Marine aerosol, sea-salt,  
816 and the marine sulphur cycle: A short review. *Atmos. Environ.* 31:73-80.
- 817 Ovadnevaite, J., O'Dowd, C., Dall'Osto, M., Ceburnis, D., Worsnop, D. R., and Berresheim, H.  
818 2011b. Detecting high contributions of primary organic matter to marine aerosol: A case study.  
819 *Geophys. Res. Lett.* 38.
- 820 Ovadnevaite, J., Ceburnis, D., Martucci, G., Bialek, J., Monahan, C., Rinaldi, M., Facchini, M. C.,  
821 Berresheim, H., Worsnop, D. R., and O'Dowd, C. 2011a. Primary marine organic aerosol: A  
822 dichotomy of low hygroscopicity and high CCN activity. *Geophys. Res. Lett.* 38.
- 823 Prather, K. A., Bertram, T. H., Grassian, V. H., Deane, G. B., Stokes, M. D., DeMott, P. J.,  
824 Aluwihare, L. I., Palenik, B. P., Azam, F., and Seinfeld, J. H. 2013. Bringing the ocean into the  
825 laboratory to probe the chemical complexity of sea spray aerosol. *Proceedings of the National*  
826 *Academy of Sciences*. 110:7550-7555.
- 827 Putaud, J., Van Dingenen, R., Mangoni, M., Virkkula, A., Raes, F., Maring, H., Prospero, J.,  
828 Swietlicki, E., Berg, O., and Hillamo, R. 2000. Chemical mass closure and assessment of the origin  
829 of the submicron aerosol in the marine boundary layer and the free troposphere at Tenerife during  
830 ACE-2. *Tellus B*. 52:141-168.
- 831 Quinn, P., and Bates, T. 2011. The case against climate regulation via oceanic phytoplankton  
832 sulphur emissions. *Nature*. 480:51-56.
- 833 Read, K. A., Mahajan, A. S., Carpenter, L. J., Evans, M. J., Faria, B. V., Heard, D. E., Hopkins, J.  
834 R., Lee, J. D., Moller, S. J., and Lewis, A. C. 2008. Extensive halogen-mediated ozone destruction  
835 over the tropical Atlantic Ocean. *Nature*. 453:1232-1235.
- 836 Reid, J. P., Dennis-Smith, B. J., Kwamena, N. A., Miles, R. E., Hanford, K. L., and Homer, C. J.  
837 2011. The morphology of aerosol particles consisting of hydrophobic and hydrophilic phases:  
838 hydrocarbons, alcohols and fatty acids as the hydrophobic component. *Physical Chemistry*  
839 *Chemical Physics*. 13:15559-15572.
- 840 Rinaldi, M., Decesari, S., Finessi, E., Giulianelli, L., Carbone, C., Fuzzi, S., O'Dowd, C. D.,  
841 Ceburnis, D., and Facchini, M. C. 2010. Primary and secondary organic marine aerosol and oceanic  
842 biological activity: Recent results and new perspectives for future studies. *Advances in*  
843 *Meteorology*. 2010.
- 844 Robinson, C. B., Schill, G. P., Zarzana, K. J., and Tolbert, M. A. 2013. Impact of Organic Coating  
845 on Optical Growth of Ammonium Sulfate Particles. *Environ. Sci. Technol.* 47:13339-13346.

- 846 Rossi, M. J. 2003. Heterogeneous reactions on salts. *Chem.Rev.* 103.
- 847 Rouviere, A., and Ammann, M. 2010. The effect of fatty acid surfactants on the uptake of ozone to  
848 aqueous halogenide particles. *Atmospheric Chemistry and Physics.* 10:11489-11500.
- 849 Rubasinghege, G., Ogden, S., Baltrusaitis, J., and Grassian, V. H. 2013. Heterogeneous Uptake and  
850 Adsorption of Gas-Phase Formic Acid on Oxide and Clay Particle Surfaces: The Roles of Surface  
851 Hydroxyl Groups and Adsorbed Water in Formic Acid Adsorption and the Impact of Formic Acid  
852 Adsorption on Water Uptake. *The Journal of Physical Chemistry A.* 117:11316-11327.
- 853 Saiz-Lopez, A., Plane, J., Mahajan, A., Anderson, P., Bauguitte, S., Jones, A., Roscoe, H., Salmon,  
854 R., Bloss, W., and Lee, J. 2008. On the vertical distribution of boundary layer halogens over coastal  
855 Antarctica: implications for O<sub>3</sub>, HO<sub>x</sub>, NO<sub>x</sub> and the Hg lifetime. *Atmospheric Chemistry and*  
856 *Physics.* 8:887-900.
- 857 Samy, S., Mazzoleni, L. R., Mishra, S., Zielinska, B., and Hallar, A. G. 2010. Water-soluble  
858 organic compounds at a mountain-top site in Colorado, USA. *Atmos.Environ.* 44:1663-1671.
- 859 Schauer, J. J., Kleeman, M. J., Cass, G. R., and Simoneit, B. R. 2002. Measurement of emissions  
860 from air pollution sources. 4. C1-C27 organic compounds from cooking with seed oils.  
861 *Environ.Sci.Technol.* 36:567-575.
- 862 Schauer, J. J., Kleeman, M. J., Cass, G. R., and Simoneit, B. R. 1999. Measurement of emissions  
863 from air pollution sources. 1. C1 through C29 organic compounds from meat charbroiling.  
864 *Environ.Sci.Technol.* 33:1566-1577.
- 865 Soule, M. C. K., Blower, P. G., and Richmond, G. L. 2007. Effects of atmospherically important  
866 solvated ions on organic acid adsorption at the surface of aqueous solutions. *J Phys Chem B.* 111.
- 867 Stemmler, K., Vlasenko, A., Guimbaud, C., and Ammann, M. 2008. The effect of fatty acid  
868 surfactants on the uptake of nitric acid to deliquesced NaCl aerosol. *Atmospheric chemistry and*  
869 *physics.* 8:5127-5141.
- 870 Sun, L., Hede, T., Tu, Y., Leck, C., and Ågren, H. 2013. Combined Effect of Glycine and Sea Salt  
871 on Aerosol Cloud Droplet Activation Predicted by Molecular Dynamics Simulations. *The Journal*  
872 *of Physical Chemistry A.* 117:10746-10752.
- 873 Sun, L., Li, X., Hede, T., Tu, Y., Leck, C., and Ågren, H. 2012. Molecular dynamics simulations of  
874 the surface tension and structure of salt solutions and clusters. *The Journal of Physical Chemistry B.*  
875 116:3198-3204.
- 876 Tabazadeh, A. 2005. Organic aggregate formation in aerosols and its impact on the  
877 physicochemical properties of atmospheric particles. *Atmos.Environ.* 39:5472-5480.
- 878 Takahama, S., and Russell, L. 2011. A molecular dynamics study of water mass accommodation on  
879 condensed phase water coated by fatty acid monolayers. *Journal of Geophysical Research:*  
880 *Atmospheres (1984–2012).* 116.
- 881 Tang, I. N., and Munkelwitz, H. R. 1993. Composition and Temperature-Dependence of the  
882 Deliquescence Properties of Hygroscopic Aerosols. *Atmospheric Environment Part A-General*  
883 *Topics.* 27.

- 884 Tervahattu, H., Hartonen, K., Kerminen, V. M., Kupiainen, K., Aarnio, P., Koskentalo, T., Tuck, A.  
885 F., and Vaida, V. 2002. New evidence of an organic layer on marine aerosols. *Journal of*  
886 *Geophysical Research-Atmospheres*. 107:4053.
- 887 Vaishya, A., Ovadnevaite, J., Bialek, J., Jennings, S. G., Ceburnis, D., and O'Dowd, C. D. 2013.  
888 Bistable effect of organic enrichment on sea spray radiative properties. *Geophys.Res.Lett.* 40:6395-  
889 6398.
- 890 Veghte, D. P., Altaf, M. B., and Freedman, M. A. 2013. Size Dependence of the Structure of  
891 Organic Aerosol. *J.Am.Chem.Soc.* 135:16046-16049.
- 892 Von Glasow, R. 2008. Atmospheric chemistry - Sun, sea and ozone destruction. *Nature*. 453.
- 893 Wagner, J., Andrews, E., and Larson, S. M. 1996. Sorption of vapor phase octanoic acid onto  
894 deliquescent salt particles. *Journal of geophysical research*. 101:19533-19,540.
- 895 Weis, D. D., and Ewing, G. E. 1996. Infrared spectroscopic signatures of (NH<sub>4</sub>)<sub>2</sub>SO<sub>4</sub> aerosols.  
896 *Journal of geophysical research*. 101:18709-18,720.
- 897 Wise, M. E., Baustian, K. J., Koop, T., Freedman, M. A., Jensen, E. J., and Tolbert, M. A. 2012.  
898 Depositional ice nucleation onto crystalline hydrated NaCl particles: a new mechanism for ice  
899 formation in the troposphere. *Atmospheric Chemistry and Physics*. 12:1121-1134.
- 900 Yassaa, N., Meklati, B. Y., Brancaloni, E., Frattoni, M., and Ciccioli, P. 2001. Polar and non-polar  
901 volatile organic compounds (VOCs) in urban Algiers and saharian sites of Algeria. *Atmos.Environ.*  
902 35:787-801.
- 903 Zangmeister, C. D., Turner, J. A., and Pemberton, J. E. 2001. Segregation of NaBr in NaBr/NaCl  
904 crystals grown from aqueous solutions: Implications for sea salt surface chemistry.  
905 *Geophys.Res.Lett.* 28.
- 906  
907

908 **FIGURE CAPTION**

909

910 **Figure 1:** Diagram of the experimental setup.

911 **Figure 2:** Representative particle size distributions of dry NaCl aerosol. Upper plot has been  
912 obtained by imaging particles deposited on a glass slide by SEM technique and counting them with  
913 the ImageJ software [rsbweb.nih.gov/ij/]. Bottom plots have been obtained by sizing particles by an  
914 aerodynamic particle spectrometer; pure NaCl particles (left) and heterogeneously nucleated  
915 particles with hexanoic particles (right) are shown.

916 **Figure 3:** Infrared extinction spectra of HA, OA and LA in different conditions: bottom spectra are  
917 from bulk phase acid; medium spectra corresponds to homogeneously nucleated acid particles;  
918 upper spectra are from heterogeneously nucleated acids onto NaCl particles. In all cases, the upper  
919 spectra have been increased for clarity (increasing factor:  $\times$ Number)

920 **Figure 4:** SEM images of: (a) pure NaCl particles; (b) pure LA particles; (c) NaCl particles covered  
921 with LA.

922 **Figure 5:** Infrared spectra of NaBr particles after passing through the heated reservoir containing  
923 OA and exposed to different RHs.

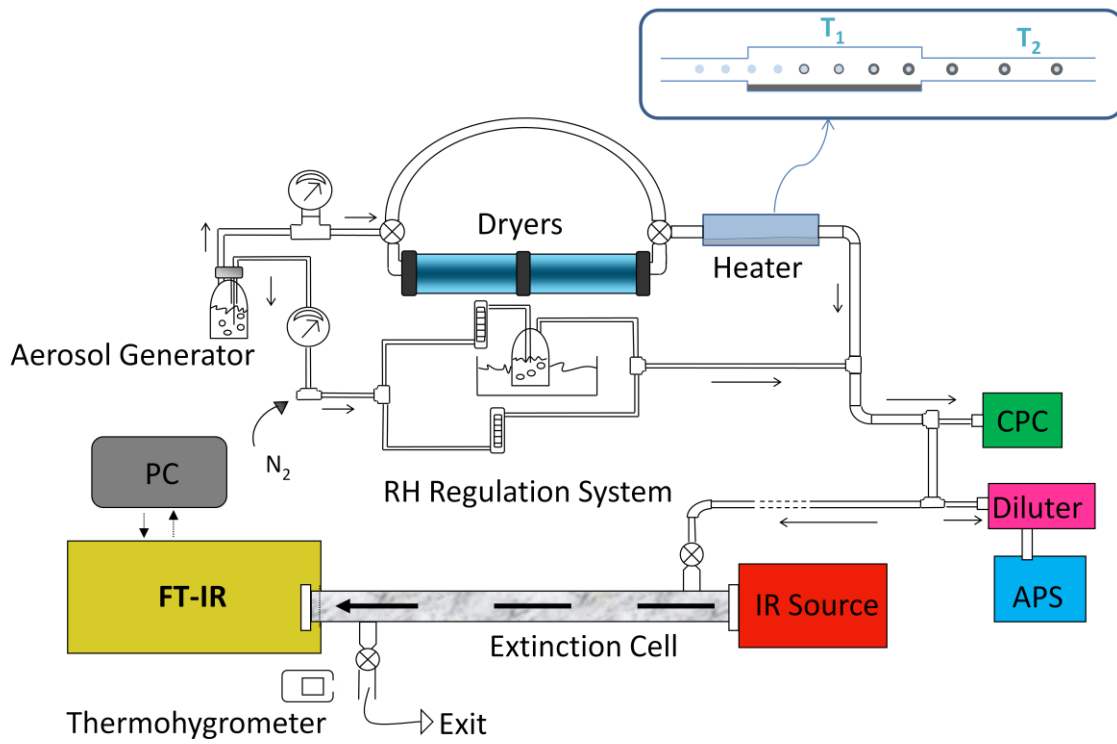
924 **Figure 6:** Evolution of the infrared absorption intensity of the C=O band of hexanoic acid with RH  
925 in NaBr particles in deliquescence and efflorescence mode. The shaded region indicates the selected  
926 area for measuring liquid water abundance in the particles (see text).

927 **Figure 7:** Deliquescence and efflorescence curves of NaX (X = Cl, Br, I) particles covered with  
928 HA, OA and LA. The curves for the pure inorganic salts are shown by lines.

929 **Figure 8:**  $N_{\text{HA}}/N_{\text{H}_2\text{O}}$  and  $N_{\text{OA}}/N_{\text{H}_2\text{O}}$  mole ratios in heterogeneously coated particles at various  
930 relative humidities in deliquescence and efflorescence conditions. “del” and “effl” stand for  
931 deliquescence and efflorescence. “RH” stands for relative humidity.

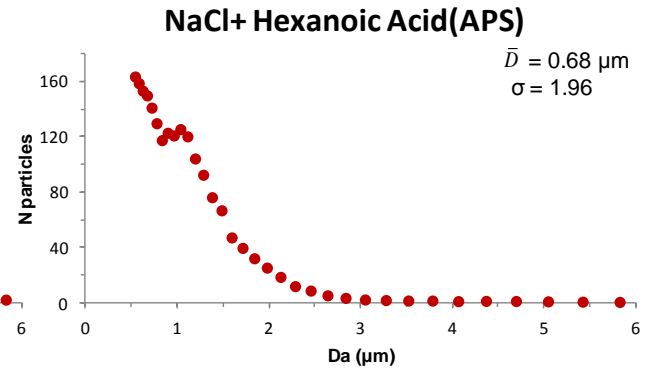
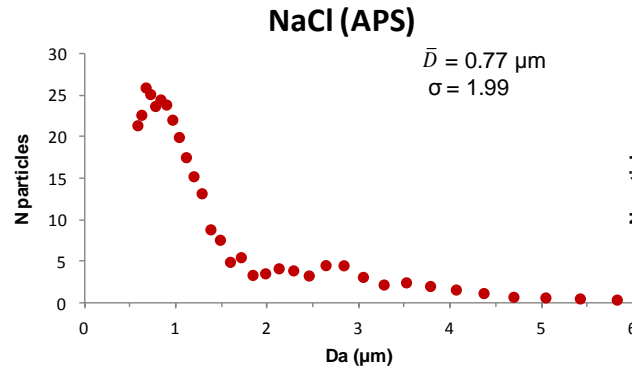
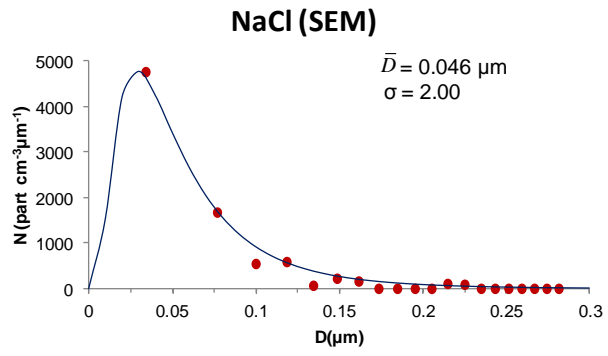
932

933 **FIGURE 1**  
934  
935



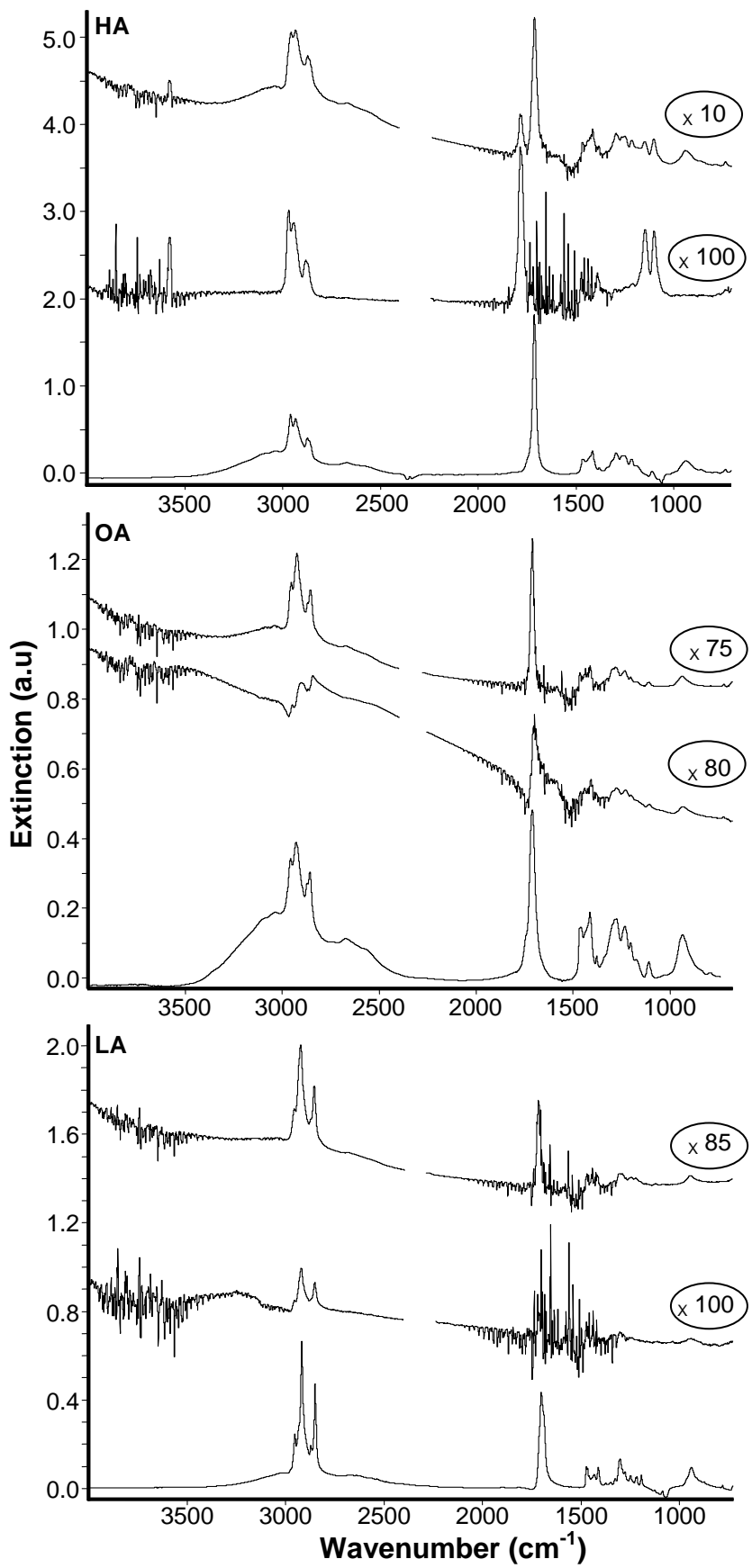
936  
937

938 **FIGURE 2**



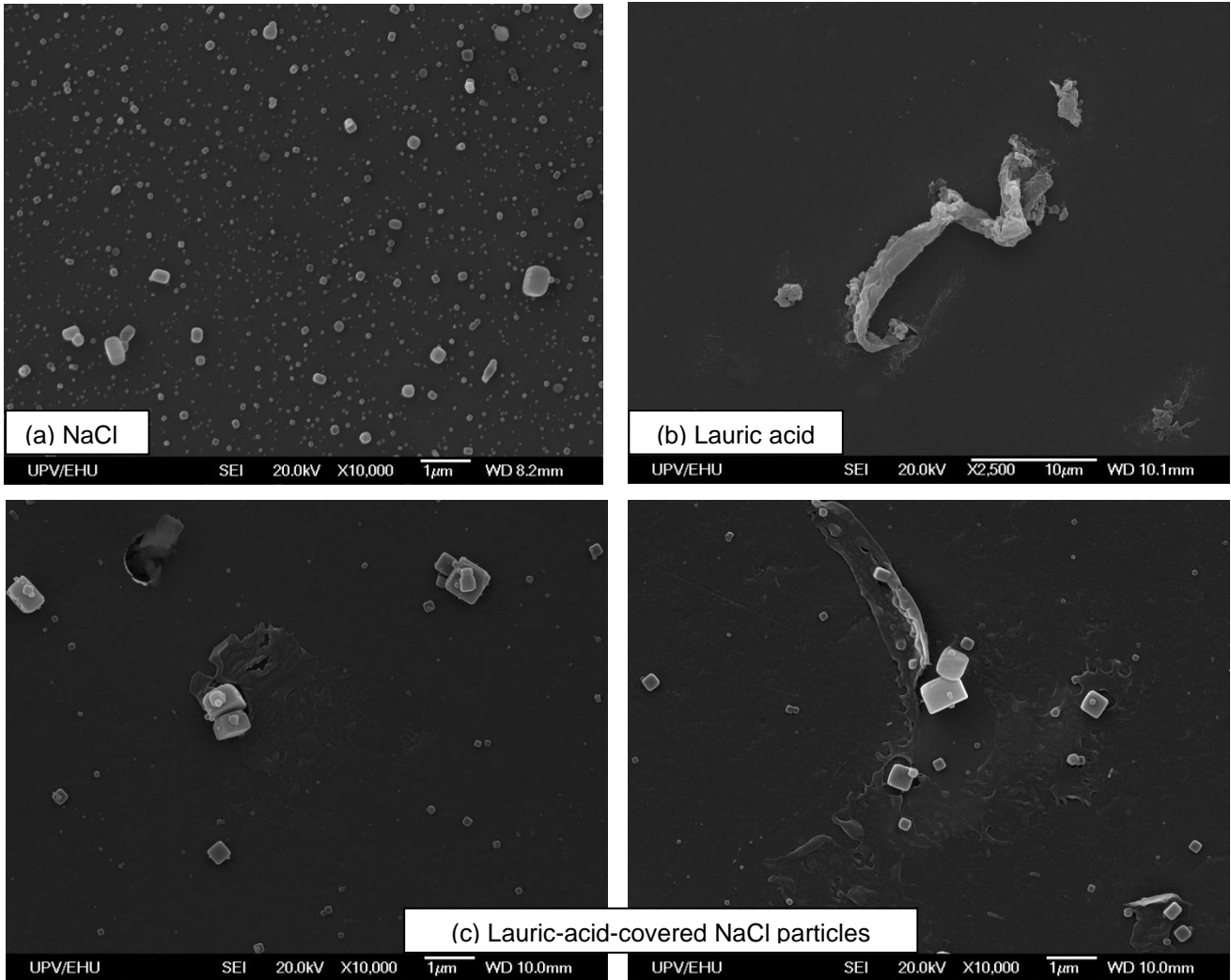
939  
940

941 **FIGURE 3**



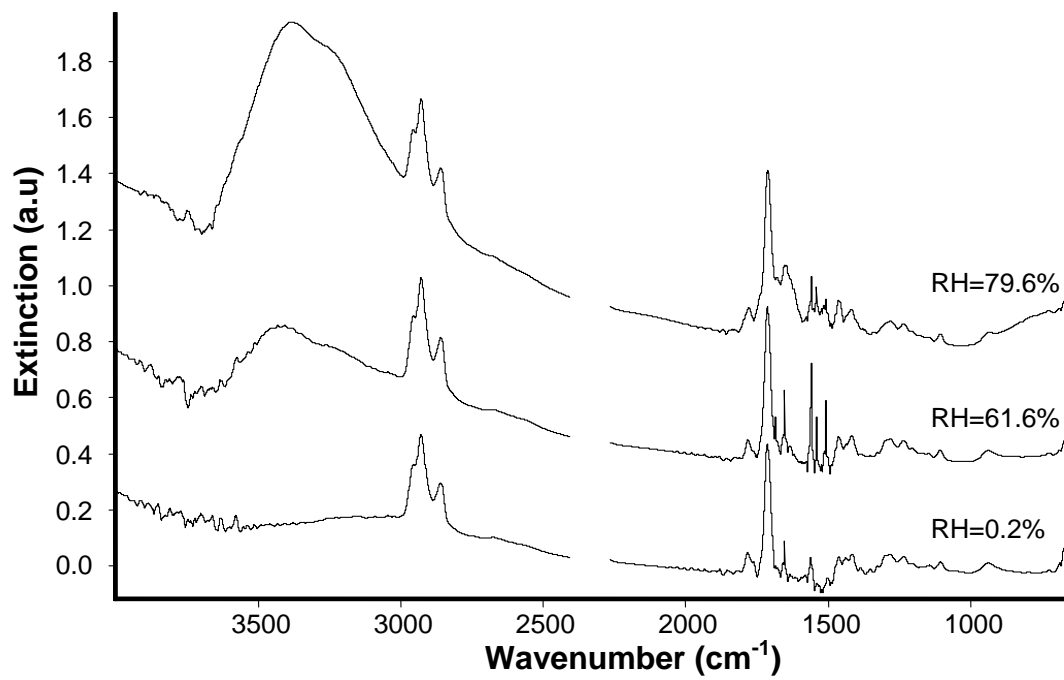


992 **FIGURE 4**  
993  
994  
995  
996

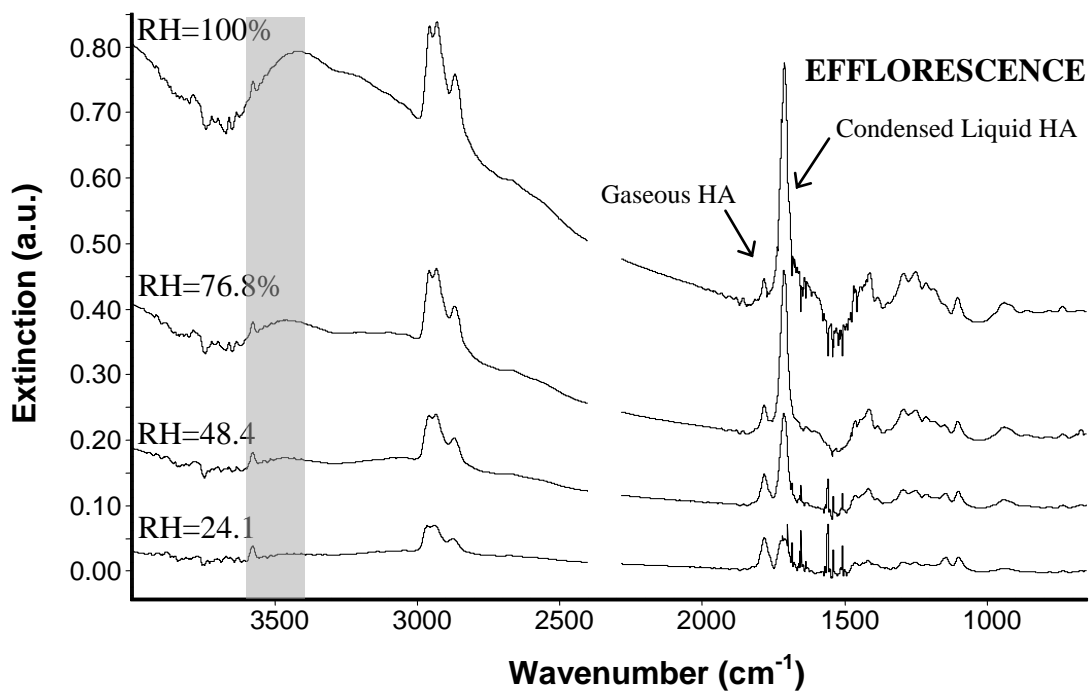
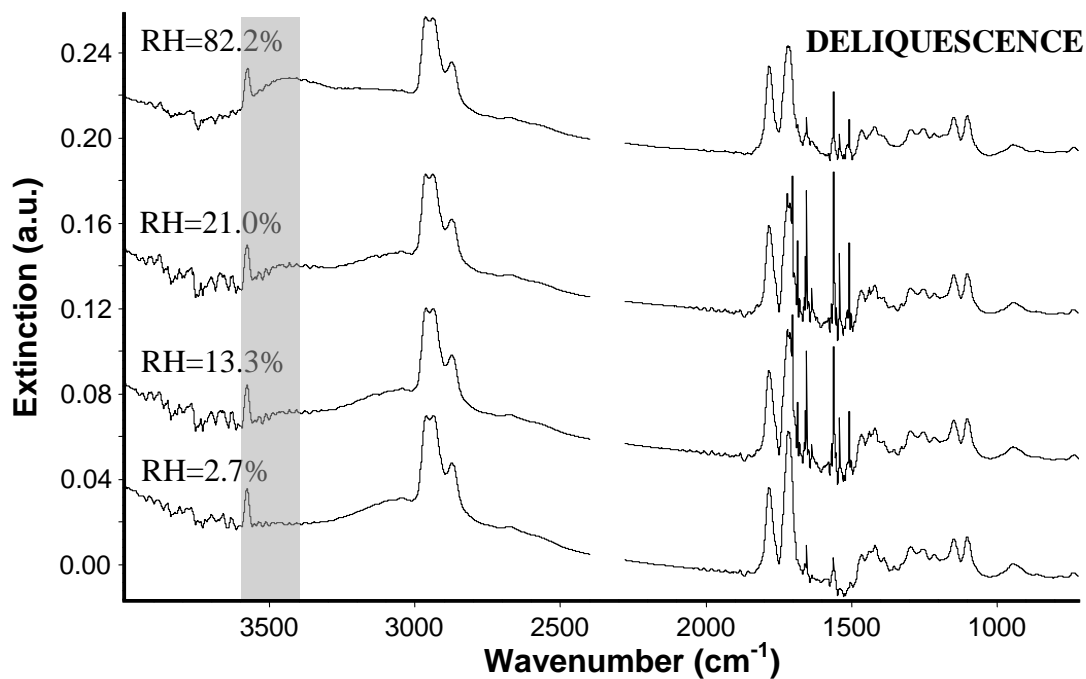


997  
998  
999  
1000  
1001  
1002  
1003  
1004  
1005  
1006  
1007  
1008  
1009  
1010  
1011  
1012  
1013  
1014  
1015  
1016  
1017  
1018

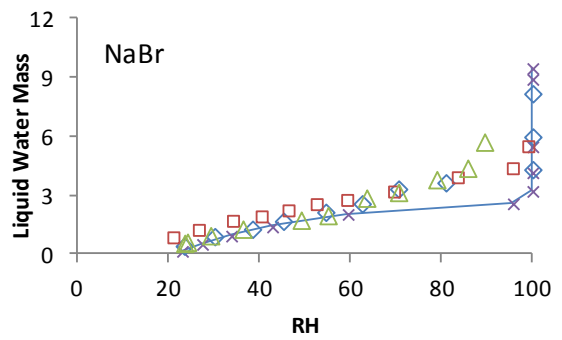
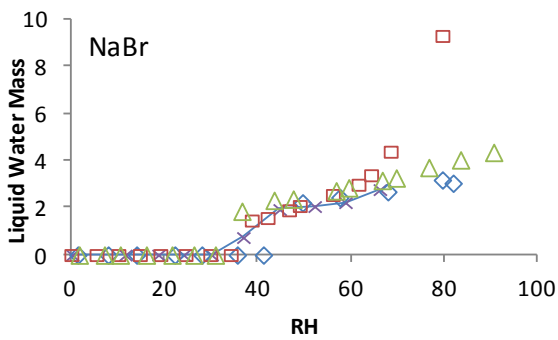
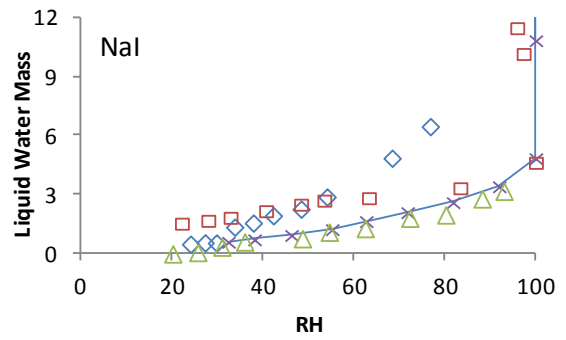
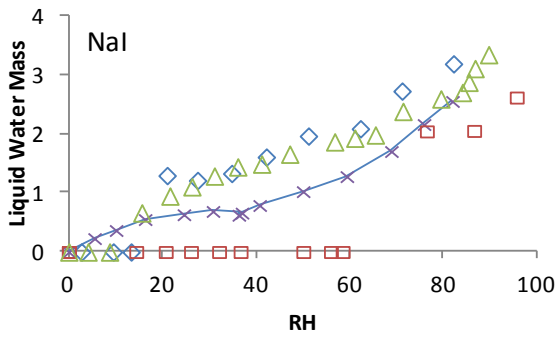
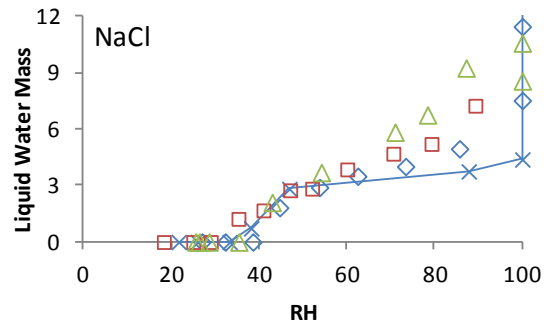
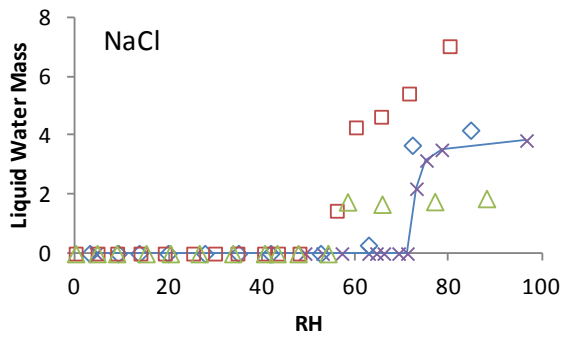
**FIGURE 5**



1019 **FIGURE 5**



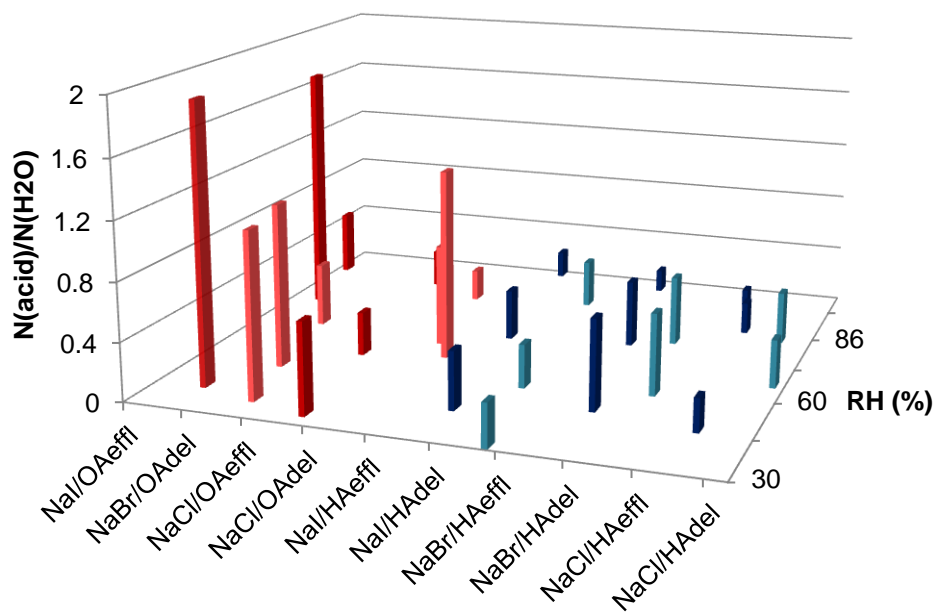
1064 **FIGURE 6**  
 1065



◆ H. A.      □ O.A.      △ L.A.      × Pure NaX

1066  
 1067  
 1068  
 1069

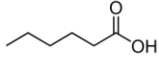
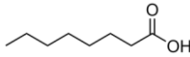
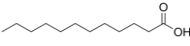
1070 **FIGURE 7**  
1071



1072  
1073

1074 **TABLE 1**  
 1075  
 1076 Physical properties of the studied carboxylic acids

1077  
 1078

Name	#C	Structural Formula	Melting Point (K) <sup>a</sup>	Boiling Point (K) <sup>a</sup>	Water solubilities (20°C, g/l) <sup>b</sup>	Vapour pressure (mbar, 25°C) <sup>c</sup>
Hexanoic Acid	6		269.7	477±4	9.9	0.272
Octanoic Acid	8		289.3±0.7	510±4	0.68	5.05×10 <sup>-3</sup>
Lauric Acid	12		317±2	571	0.058	2.18×10 <sup>-5</sup>

1079

1080 **a:** NIST Chemistry WebBook

1081 **b:** The Merck Index: An encyclopedia of chemicals, drugs and biologicals (11th Ed.), Merck, 1989

1082 **c:** PubChem Compound, NCBI (National Centre for Biotechnology Information)

1083

1084

1085

1086

1087 **TABLE 2**  
 1088  
 1089 Band position and bandwidth of the C=O stretching band in various conditions for HA, OA and LA.  
 1090 Units in cm<sup>-1</sup>

	Hexanoic acid		Octanoic acid		Lauric acid	
	Wavenumber at maximum intensity	Bandwidth (FWHM)	Wavenumber at maximum intensity	Bandwidth (FWHM)	Wavenumber at maximum intensity	Bandwidth (FWHM)
gas <sup>a</sup>	1780	26	1780	62	1790	30
bulk	1710	20	1713	26	1700	29
homog. nucl.	1730	26	1700	46	1710	21
heter. NaCl <sup>b</sup>	1717	27-40 <sup>c</sup>	1707	19	1710	19
heter. NaBr <sup>b</sup>	1711-1720 <sup>c</sup>	27-37 <sup>c</sup>	1713	23	1708	26
heter. NaI <sup>b</sup>	1720	33	1713	36	1707	13

- 1091  
 1092 <sup>a</sup> NIST Chemistry Webbook: <http://webbook.nist.gov/chemistry>  
 1093 <sup>b</sup> Dry particles  
 1094 <sup>c</sup> Depending on the amount of acid deposited onto the salt particles